Groundwater dynamics in a hydrologically-modified alpine watershed from an ancient managed recharge system (Sierra Nevada National Park, S Spain): insights from hydrogeochemical and isotopic information

Barberá, J.A.[1], Jódar, J.[2,3,*], Custodio, E.[2,5], González-Ramón, A.[4], Jiménez-Gavilán, P.[4], Vadillo, I.[1], Pedrera, A.[4], Martos-Rosillo, S.[4]

[1] Centre of Hydrogeology of the University of Málaga (CEHIUMA), Spain

[2] Groundwater Hydrology Group, Dept. Civil and Environmental Eng., Technical University of Catalonia (UPC)

[3] Hydromodel Host S.L. and Aquageo Proyectos S.L., Spain

[4] Department of Ecology and Geology, University of Málaga, Spain

[5] Geological and Mining Institute of Spain (IGME), Spain

[6] Royal Academy of Sciences of Spain, Spain

*Corresponding author: Jorge Jódar (jorge.jodar@hydromodelhost.com). Ph: (+34) 619712122

Abstract

In the alpine watersheds of Sierra Nevada National Park (Southern Spain), water resources from rivers and streams are used as a supply of drinking water for human settlements, for irrigation in agriculture, and for the maintenance of dependent ecosystems. The hydrologic functioning of many of these rivers and streams has been artificially modified, at least since the Middle Ages, by means of a dense network of dug canals (locally known as *acequias de careo*) employed to recharge water from snowmelt

in the uplands. Recharged water from the channel system emerges downstream, in springs and along the riverbed in the lower catchment area, but delayed in time. This ancient practice guarantees the water needs for dispersed mountain settlements and for irrigation of their croplands during the dry season. In this paper, an initial evaluation of the recharge rate in the studied aquifer accounts for 15-20% of the mean annual precipitation, while 69-97% of the total discharge in the Bérchules River watershed (BRW) is groundwater contribution to surface runoff, which is linked to the effectiveness of the ancient managed aquifer recharge technique. The altitude difference between the natural and artificial recharge system areas and the discharge zones is the main factor responsible for the observed changes in the isotopic composition of groundwater. Moreover, the mechanisms for mineralization of groundwater are based on geochemical processes such as evapo-concentration in the soil layer and silicate mineral weathering due to dissolved CO_2 from the soil and the atmosphere. The marked NO_3^- enrichment of groundwater throughout the BRW and around urban settlements reflects the influence of agriculture and wastewaters on its chemical status. Our study considers the benefits of the ancient *acequias de careo* water management system as a tool to extend the availability of water resources during the dry season. This is of interest in similar mountainous settings, particularly to mitigate the possible negative impact of climate change on the population and livelihoods in downstream areas.

Keywords:

Alpine watershed; Aquifer managed recharge; Hydrogeochemistry; Isotope hydrology; Extended water resources; *Acequia de careo*

1. Introduction

Water from high mountains, known as "water towers", generates 30% of the global discharge (Meybeck et al., 2001). This role is even more important in semiarid and arid zones, where its contribution varies between 50% and 90% (Messerli et al., 2004; Viviroli et al., 2007). Meltwater from “water towers” is essential not only for human sustenance, but also to maintain associated downstream ecosystems and enhance their ecological diversity (Beniston et al., 1997). Yet these hydrological systems are vulnerable to the impact of climate change (Immerzeel et al., 2010). The early effect of an ongoing global climate change has been observed in terms of glacial recession in the world’s highest mountain systems, including the Andes (Fraser, 2012), the Himalayas (Scherler, 2011), the Rocky Mountains (Moore et al., 2009) or the Alps (D’Agata et al., 2014), among others. From the perspective of high mountain hydrological basin behavior, the increasing temperatures that are currently observed may well lead to earlier runoff in spring or winter, and to reduced discharge in summer or autumn (Barnett et al., 2005, and references therein). Nevertheless, assessment of the most likely impact of climate change on such high mountain hydrological basins calls for historical characterization. This is no easy task given the difficulty of access, the adverse working conditions and the type of instruments required for measuring hydrological variables in high mountain zones (Clow et al., 2003; Langston et al., 2013; Molina et al., 2014; Hood and Hayashi, 2015).

A great effort therefore goes into characterizing high mountain hydrological systems, and especially the aquifers located in these physiographic settings. The water they store can be used to alleviate the potentially adverse effects of climate change (Viviroli et al., 2011; Taylor et al., 2012). The study of such hydrological systems typically involves a multidisciplinary approach that combines data from different information sources: geophysical (McClymont et al., 2010, 2012), hydrological (Kahn et al., 2008; Liu et al.,

2008; Roy and Hayashi, 2009; Lauber et al., 2014; Chen at al., 2017), and geochemical and environmental isotopes (Lauber and Goldscheider, 2014; Lambán et al., 2015; Herrera et al., 2016; Jódar et al., 2016). Processes such as snow accumulation and melting, as well as groundwater discharge, would play a major role in the dynamics of such alpine hydrological systems. A number of authors report high groundwater discharge with respect to the total alpine basin runoff (Clow et al., 2003; Huth et al., 2004; Liu et al., 2004; Hood et al., 2006; Cras et al., 2007; Jódar et al., 2017) in high slope areas with presumably low-permeability hard rock substrates. This fact highlights the importance of groundwater contribution in the behavior of high mountain rivers, which is even more relevant when they are located in semi-arid environments, given that groundwater provides a critical resource downstream by sustaining river base flow during long-lasting dry periods.

This paper explores the functioning of the Bérchules River Watershed (BRW), an alpine hydrologic system where the groundwater component feeding the total basin discharge is anomalously high (Jódar et al., 2017, 2018). The study area is located along the southern edge of Sierra Nevada (S Spain), which is the highest mountain range of the Iberian Peninsula. Despite its altitude, the mountainous system is fully de-glaciated since the middle of the past century (Gómez-Ortiz et al., 2012, 2015), a process most likely accelerated by the semi-arid climate conditions prevailing in the region (Gómez-Zotano et al., 2015). The southern edge of Sierra Nevada has been colonized for many centuries (Martín-Civantos, 2007). In this area, an ancestral water management system, operative to date, was designed to supply water to the local population for domestic use, crop irrigation and cattle. The artificial water management system is known in Spanish as "*acequias de careo*", and constitutes a means of artificially recharging the aquifer with snowmelt by means of long channels excavated in the terrain (Pulido-Bosch and Sbih,

1995; Martos-Rosillo et al., 2017). The recharge system is so efficient and resilient that it has been maintained, with very few modifications, at least since the Middle Ages (Delaigue, 1995).

The main objective of this work is to investigate the role played by this ancestral water management system in the hydrologic behavior of the BRW. A multidisciplinary approach is adopted by integrating basin hydrodynamic data with groundwater geochemistry and its isotopic composition. From data integration, a conceptual model of the hydrological basin is established and, furthermore, recharge to the underlying aquifer has been estimated.

2. General setting

BRW is located at the southern edge of the Sierra Nevada mountain range (Granada province, S Spain; Fig. 1); it is approximately 30 km away from the Mediterranean coast, where it outflows, changing its name to the Guadalfeo River. The study area covers a rugged land surface of 68 km^2, with conspicuously asymmetric V-shape valleys dug by the river network. The average slope is 37%. The average altitude is 2070 m a.s.l. (above sea level), topping at ~2900 m a.s.l. at the north of the watershed, while the lower altitude zones (<1000 m a.s.l.) coincide with the southern border of the BRW, where the gauging station of the Bérchules River is located (Narila station; S8 in Fig. 1B). The soil cover is mainly represented by sparse scrub crops, conifers and grassland adapted to low temperatures and low humidity, as well as by fruit trees and irrigated horticulture crops, particularly in the lowlands —but also in a reduced area in the uplands— amounting to about 260 hectares (4% of the total catchment surface area).

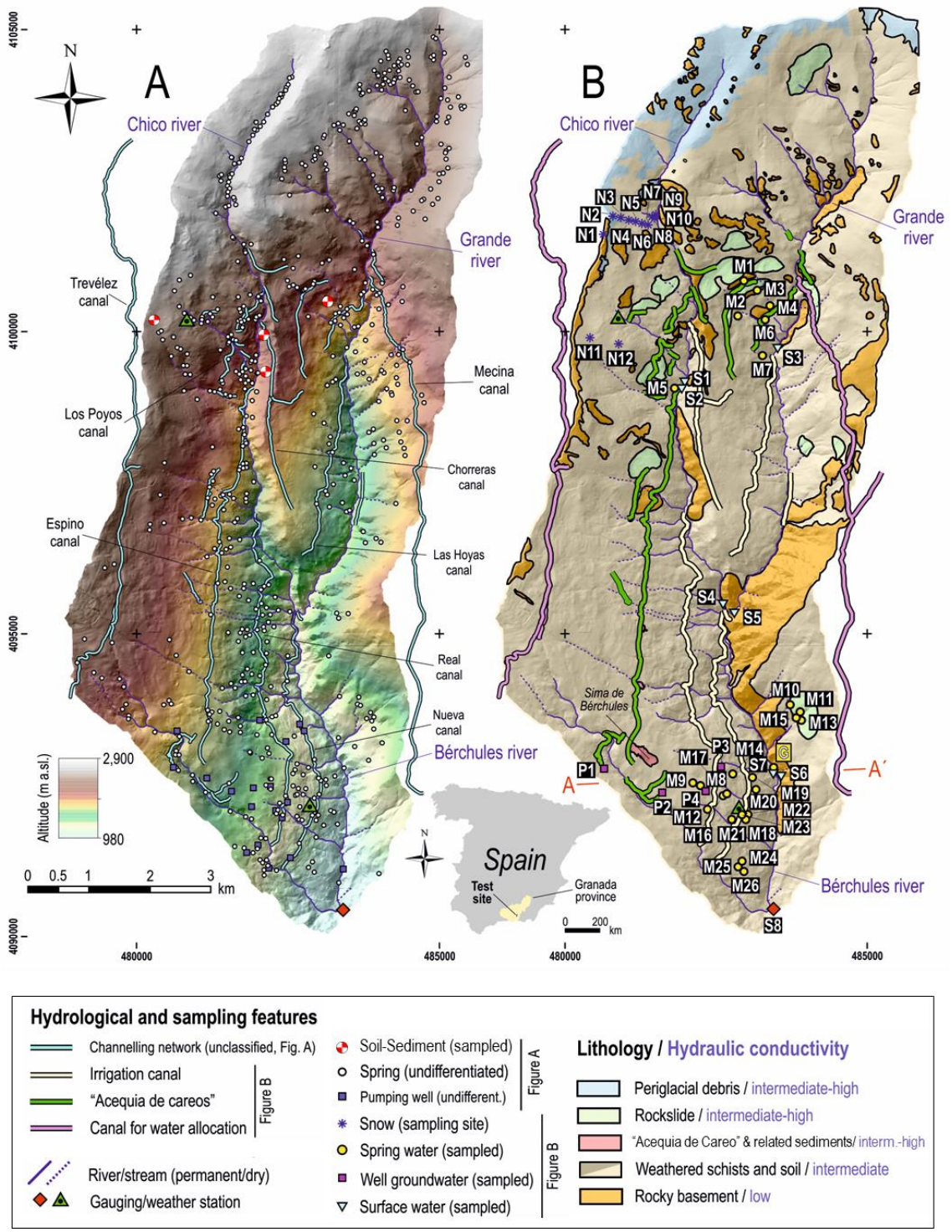

120

121 **Figure 1:** Location map, altitude, and spatial distribution of soil sampling points and
122 springs (A) with geological map (B) of the Bérchules River Watershed (BRW). The labels
123 of the water sampling points correspond to those in Table 1.

124

125 The climate of the study area is continental. At the Bérchules meteorological station (Fig.
126 1), the average values of precipitation (P), temperature (T) and potential
127 evapotranspiration (ETP) calculated with the Hargreaves (1994) formula are 828 mm/yr,
128 12.9 °C and 1033 mm/yr, respectively. These three variables show a seasonal variation
129 (Fig. 2) and elevation dependence (Jódar et al., 2017). The vertical gradients of
130 precipitation (∇_zP), temperature ($\nabla_z T_{atm}$) and potential evapotranspiration (∇_zETP) are
131 22.2 mm/yr/100 m, −0.62 °C/100 m and −24.9 mm/yr/100 m, respectively. The snow cap
132 is almost permanent in the upper zones of the basin, meaning that precipitation is partly
133 produced as snow. This is reflected in the Bérchules River hydrograph, which shows a
134 discharge peak during the spring season (Fig. 2) corresponding to snowmelt runoff (Jódar
135 et al., 2017).

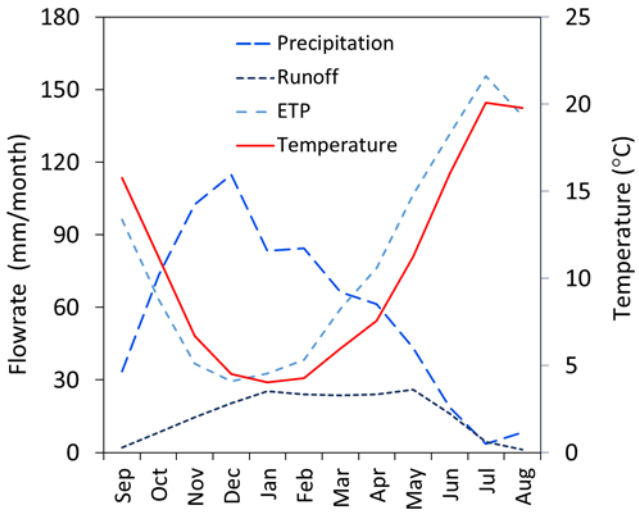

136

137 **Figure 2:** Seasonal variation of precipitation, potential evapotranspiration, Bérchules
138 River runoff (measured at the Narila gauging station; Fig. 1) and temperature.

139 Studied site is located in the Nevado-Filábride Complex, which in turn belongs to the
140 Internal Zone of the Betic Range (e.g. Aldaya et al., 1979, 1983). The rocks are Palaeozoic
141 in age and were subjected to subduction and exhumation during the Miocene, recording
142 ductile deformation and metamorphism. The BRW is mostly floored by graphite schists

143 with feldspar, garnet and chloritoid minerals, interbedded quartzites, and local marble and
144 amphibolite lenses that contain albite, glaucophane, chlorite, actinolite, and tremolite,
145 among other minerals.

146 The main ductile fabric is a penetrative foliation in the schists mostly containing
147 muscovite, chloritoid minerals and quartz, which in the BRW generally dips to the N-NE.
148 The main foliation is locally deformed and converted into late open joints that are
149 frequently filled by iron oxides. In some specific sectors, the uppermost 30-50 m of the
150 graphite schists show intense alteration. Two different alteration zones can be
151 differentiated: an upper highly weathered schist zone and a lower fractured/fissured schist
152 zone (Martos-Rosillo et al., 2017). Quaternary deposits of diverse origin (glacial, alluvial,
153 soil sliding, periglacial debris and alluvial fan sediments) overlie the metamorphic rocks,
154 mainly in the uplands, where the topography is smoothed.

155 The Bérchules River and its tributary branches (Chico and Grande rivers) are the main
156 hydrologic features in the study area (Fig. 1). The river has a pluvio-nival hydrologic
157 behavior, with maximum discharge in January-May and minimum flow during July-
158 September (Fig. 2). The mean annual runoff is estimated to be 13.1 hm^3/year for the
159 period 1970-2013, groundwater contribution representing more than 90% of the total
160 basin runoff (Jódar et al., 2017).

161 The study area features the ancient but sophisticated hand-made hydraulic facility of
162 canals, including the recharge ones or *acequias de careo* mentioned in the introduction,
163 comprising a dense and complex open dug channel network. This network is used for two
164 purposes: (1) to recharge the snowmelt runoff generated in river basin uplands into the
165 subsurface; and (2) to convey river surface water to the lowlands, for crop irrigation
166 during the growing season. The recharge canals allow the infiltration of the basin

167 headwaters into the subsurface during the snowmelting-season (April to June) (Pulido
168 Bosch and Sbih, 1995; Martos-Rosillo et al., 2015a). In the BRW, the channel network
169 for water management comprises 19 canals, with a total length of 57.5 km. They are active
170 from November-December to September-October (Fig. 3).

171 In previous research conducted in the BRW during the hydrologic year 2014-2015
172 (Martos-Rosillo et al., 2017), a total discharge of 5.3 hm^3 was measured in the Bérchules
173 River at the Narila gauging station (S8 in Fig. 1). Between January and May 2015, flow
174 rate measurements were taken in the "El Espino", a 7.5 km-long main recharge canal.
175 The total water infiltration along this canal was 2 hm^3, 1.65 hm^3 corresponding to leakage
176 along the channel and 0.35 hm^3 to concentrated water infiltration at the end of the canal
177 through a sink called "Sima de Bérchules" (Fig. 1). This feature is a small fractured
178 outcrop marking a high vertical permeability zone. The larger the runoff infiltration, the
179 longer the duration of spring discharge. Once snow melting vanishes, the use of the
180 recharge canals stops and the river runoff water is derived towards the irrigation canals.
181 These irrigation canals run almost parallel to the Bérchules River at a lower altitude than
182 the recharge channels. The irrigation canals operate from April-June to September-
183 October, coinciding with the growing season in the croplands (Fig. 3).

184 From a hydrogeologic point of view, the metamorphic weathered zone along with the
185 cover of Quaternary formations would constitute a mixed granular-hard rock aquifer
186 having a total permeable surface area of 59.2 km^2 which practically accommodates that
187 of the watershed, and a variable thickness of 30-50 m (Martos-Rosillo et al., 2015a; b).
188 Once rainfall runoff and snowmelt infiltrate, the water flows as subsurface runoff towards
189 the underlying water table. The subsurface runoff may flow sub-horizontally and be
190 discharged as overland flow through the 609 springs inventoried, about 9 springs/km^2.
191 These springs generally yield $\leq$ 0.2 L/s and have an intermittent discharge regime. They

192 are mostly located in the higher parts of the watershed (Fig 1). The springs are associated
193 with (1) abrupt changes in the land slope, (2) reduced thickness of the weathered zone,
194 and (3) water leakage from the canal network (González-Ramón et al., 2015). Thus, the
195 spatial distribution of the springs accommodates the natural slopes of the massif before
196 discharging into the Bérchules River and its tributaries. In addition, deep regional
197 groundwater discharge linked to the main fracture system of the deep unaltered
198 metamorphic basement is observed in some iron-rich springs that discharge ≤ 0.2 L/s.

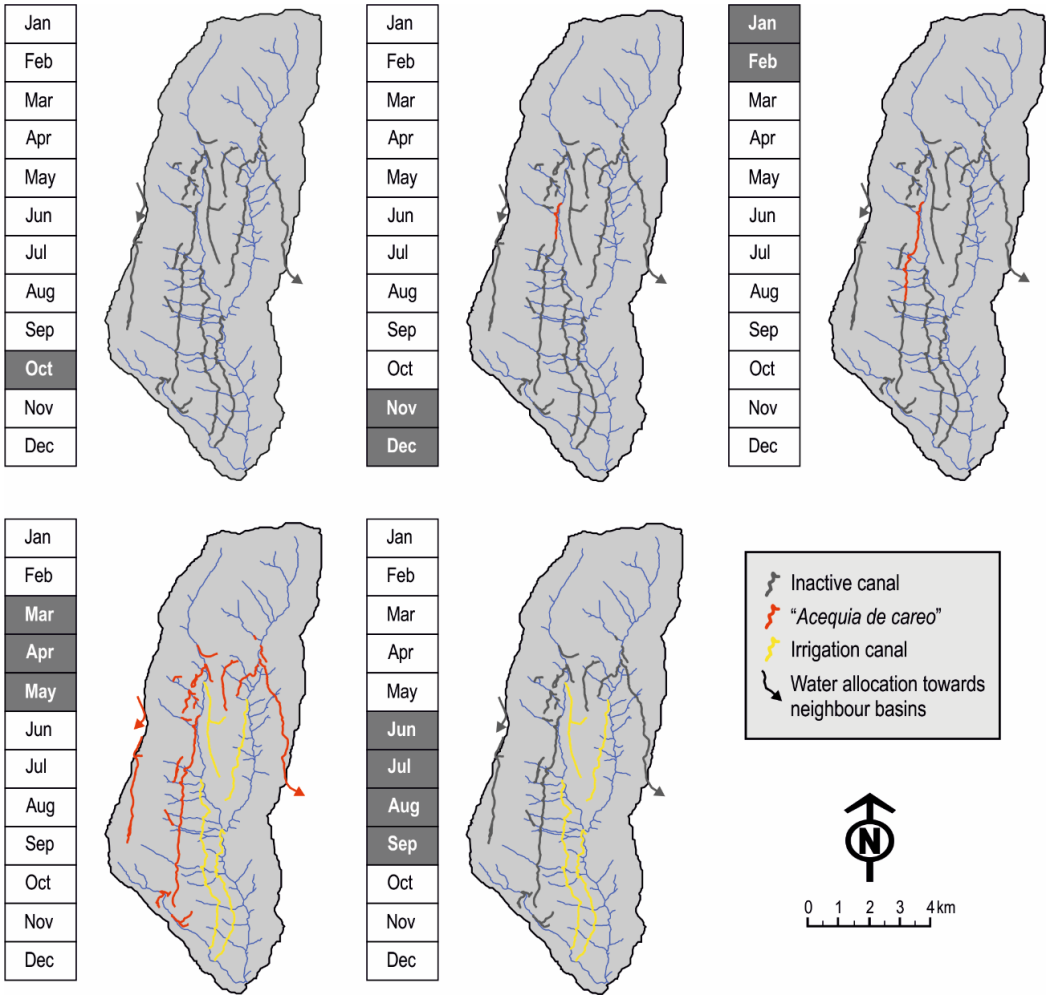

199

200 **Figure 3:** Simplified scheme of the seasonal functioning of the man-made channel
201 network (*acequias de careo* and irrigation canals) in the BRW. Canals in black do not
202 work in the indicated season and do work when in color. In blue, the natural river channel
203 network.

There are only 20 pumping wells in the basin, with pumping rates between 0.5 and 1 L/s. These wells are located in the lower part of the basin and are used to supply farming and irrigation needs in private lands. Agriculture in the BRW may play a significant role from the standpoint of groundwater quality, as is shown later.

3. Materials and methods

Two field campaigns were performed in January-February (rainy/snowy season) and May-June (snow-melting season) of 2015 for physical-chemical data acquisition through water sample collection at selected monitoring points (Fig. 1). The selection was based on permanent springs, private wells and strategic points of the hydrologic network. Discrete field measurements of electrical conductivity (EC), water temperature and pH were performed in spring waters and groundwater from pumping wells, as well as in surface water from the Bérchules River and the tributary streams. A portable electrical conductivity (EC) and temperature probe (WTW® 340i) and pH-meter (WTW® 315i) were used for measurements of field parameters. The accuracy was ±0.5% for EC and ±0.03 units for pH. Borosilicate dark glass bottles with screw caps (125 ml) containing few ml of 10% nitric acid solution (to reach pH < 2) were carefully filled with water aliquots avoiding air bubbles trapping and, therefore, sample degassing. A specific survey was conducted at the beginning of April 2015 for snow sampling in the upper part of the BRW, between 2450 and 2830 m a.s.l. Snow samples were gathered drilling through the whole snow package (Lambán et al., 2015) at different locations (Fig.1). The resulting snow samples were stored in sealed plastic bags and finally melted to obtain a representative aliquot. The analytical procedure was the same as for the rest of water samples. EC values of the melted snow water samples were computed using

228 PHREEQC™ software (Parkhurst and Appelo, 1999), assuming a water temperature of
229 4.3 ºC and a pH of 6.5, to make up for the lack of field measurements.

230 Analytic determinations of the water samples were conducted by the laboratory of the
231 Center of Hydrogeology at the University of Málaga within 48 hours after sampling.
232 Major chemical elements (Na^+, K^+, Ca^{+2}, Mg^{+2}, Cl^-, NO_3^- and SO_4^{-2}) were measured by
233 high pressure ionic chromatography (HPIC; METROHM® Compact 881 IC Pro), with an
234 accuracy of ± 2%. Alkalinity (HCO_3^- as dissolved inorganic carbon, DIC) and TOC (total
235 organic carbon) were determined using a carbon analyzer (SHIMADZU® V_{TOC}), after
236 treatment with HCl and combustion of the sample. The $\delta^{18}O$, $\delta^{2}H$ and $\delta^{13}C_{TDIC}$ (total
237 dissolved inorganic carbon) in water were measured using two cavity ring-down laser
238 spectrometers: PICARRO™ CRDS L2120-*i* for O and H isotopes and PICARRO™ CRDS
239 G2201-*i* coupled to an AURORA™ OI 1030W TOC analyzer for C isotopes. The isotope
240 data for $\delta^{18}O$ and $\delta^{2}H$ were presented in reference to the Vienna-Standard Mean Ocean
241 Water (VSMOW) and the $\delta^{13}C_{TDIC}$ in relation to the Vienna-Pee Dee Belemnite (VPDB)
242 standards. The accuracy of isotope measurements was ± 0.1‰ for $\delta^{18}O$ and ± 1‰ for
243 both $\delta^{2}H$ and $\delta^{13}C_{TDIC}$.

244 The chemical composition of soil was determined by Locutura et al. (2012) from 87 soil
245 and river bed sediment samples of different basin locations (Fig. 1). Analytical
246 measurements were conducted in the Laboratories Actlabs of Ontario (Canada). A large
247 number of chemical components including S, P, Ca, Mg, Na, K, Fe, Mn and Al were
248 measured by Inductively Coupled Plasma Atomic Emission Spectroscopy (ICP-AES)
249 techniques, which provide reliable quantitative multi-element analyses at trace levels with
250 accuracies of ± 0.01 ppm.

251

4. Results

4.1 Soil chemical data

The soils in the study area contain mostly silicate minerals such as albite, anorthite, epidote, actinolite and tremolite, but quartzite, calcite and dolomite horizons are also found. The chemical composition of the analyzed soil samples is consistent with the described mineralogical composition (Fig. 4A). The soil samples are of a kaolinite-clay dominated nature, with Ca and Mg as the main soluble elements contained in them (Fig 4B).

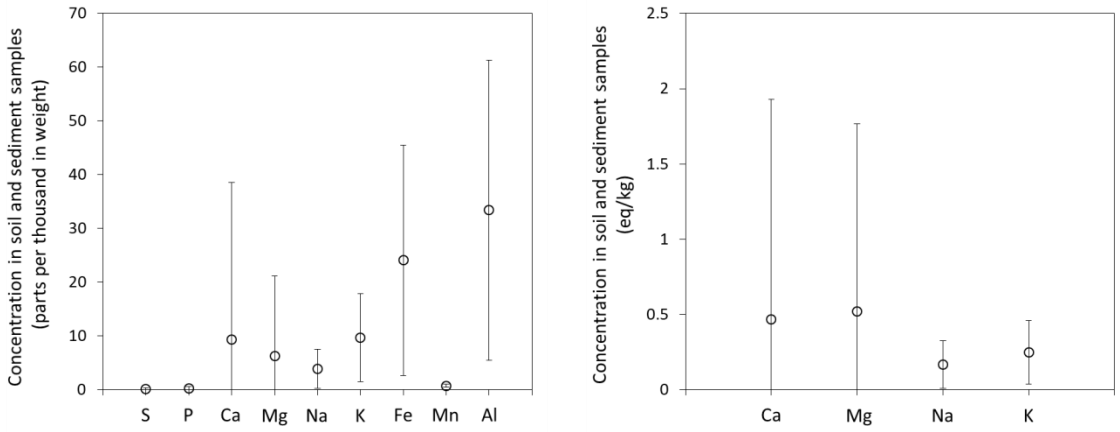

Figure 4: Major elements in soil chemical composition. Concentrations are in parts per thousand (g/kg) (A) and equivalent/kg (B).

4.2 Hydrogeochemical data

The snow samples collected in the uplands of the BRW have the weakest water mineralization (EC ≤ 36 µS/cm) (Table 1). Surface water EC values range between 15 µS/cm (S1) and 114 µS/cm (S8). The mean water temperature is 7.6 ± 3.3 ºC (5.3 ± 1.1

ºC and 10.6 ± 2.8 ºC, respectively, for the January-February and the May-June sampling campaigns). The EC in groundwater ranges between 19 and 1188 µS/cm (Table 1), with average and standard deviation values of 111 and 206 µS/cm, respectively. Such variability is spatially conditioned, given that no substantial differences in EC are observed in the monitored springs and wells between the two sampling campaigns. The average groundwater temperature and pH are respectively 12.8 ± 2.3 ºC and 7.0 ± 0.5. Groundwater sampled in spring G was found to be the most mineralized, acidic and warmest of all the sampled spring waters (Table 1 and Fig. 1).

The groundwater samples are of the calcium-bicarbonate or calcium-magnesium-bicarbonate type, although in some particular springs and wells two different hydrogeochemical facies are seen: calcium–magnesium–bicarbonate–sulphate composition and sodium–calcium–bicarbonate composition. The higher groundwater mineralization corresponds to groundwater samples taken from either deep pumping wells (e.g. P1; Table 1 and Figs. 1 and 5) or springs discharging regional groundwater flow lines (e.g. Spring G). While snow samples have a calcium bicarbonate-sulphate hydrochemical facies, the majority of surface waters and groundwater are of the calcium-magnesium bicarbonate-sulphate type (Fig. 5). Organic-derived chemical compounds as TOC and NO_3^- were detected generally in low concentrations, with maximum values of 11.8 mg/L (M15) and 14.5 mg/L (M19), respectively (Table 1 and Fig. 1). The average TOC and NO_3^- contents are similar in snow and surface waters, but much higher in groundwater (both springs and wells and the two sampling campaigns), along the order of 2-3 times for TOC and 5 times for NO_3^-.

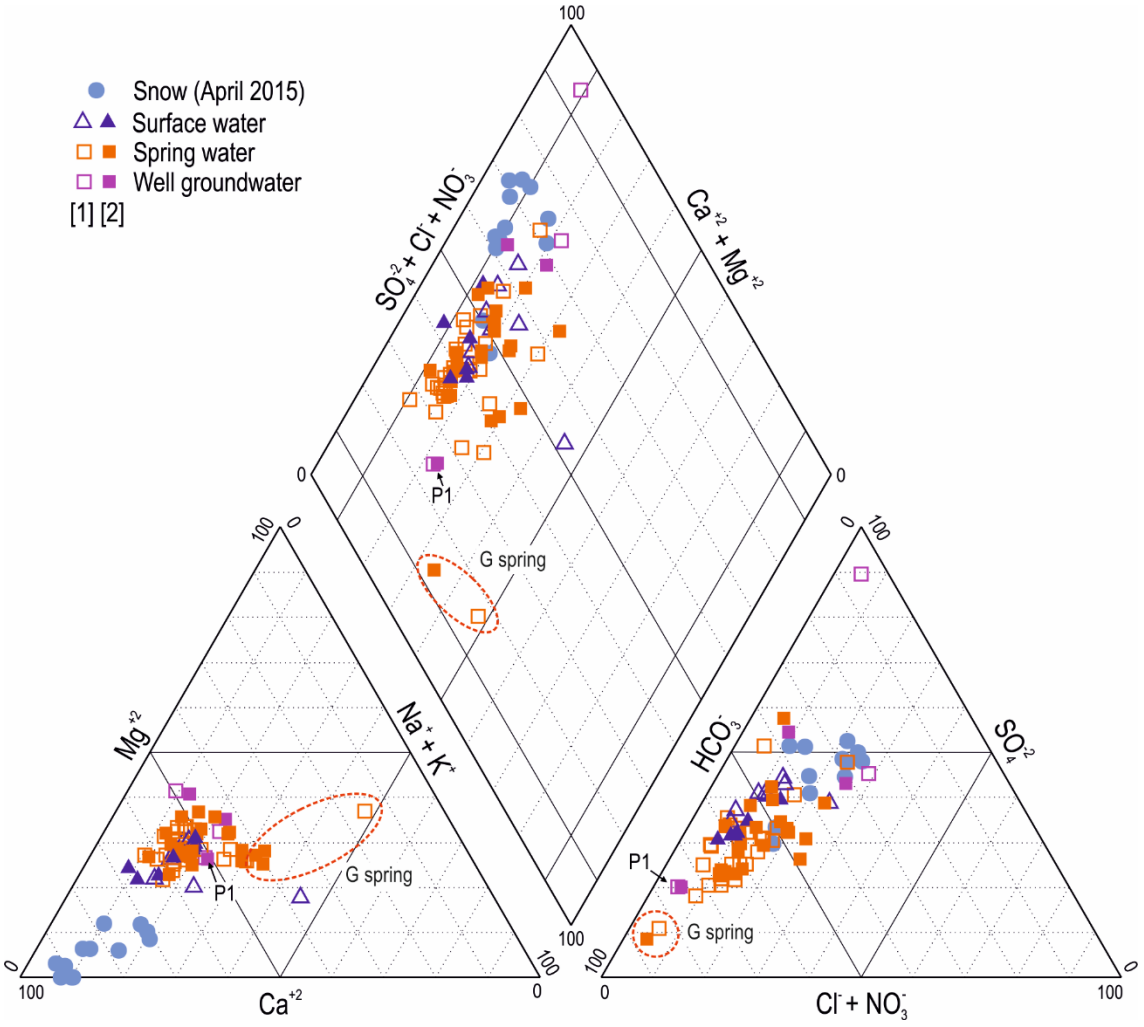

Figure 5: Compositional (Piper) diagram showing the hydrochemical facies of the waters sampled in the BRW. Numbers in brackets refer to January-February [1] and May-June [2] field surveys.

Table 1. Chemical and isotopic data of snow, spring water, surface water and groundwater well samples collected in BRW during January-February (J-F) and May-June (M-J) field surveys in 2015 (snow samples were collected in April 2015). Analytical determinations: electrical conductivity data of snow water computed using PHREEQC™ (Parkhurst and Appelo, 1999); alkalinity (*) expressed as HCO_3^-; bdl: below detection limit; (-) not determined. Values are in mg/L if not otherwise indicated.

Ref.	Water type	Elevation	Discharge		Elect. Cond.		Temperature		pH		TOC		Na^+		K^+		Ca^{+2}		Mg^{+2}		Alkalinity*		Cl^-		NO_3^-		SO_4^{-2}		δ^2H		$\delta^{18}O$		*d* excess		$\delta^{13}C_{DIC}$	
		[m a.s.l.]	[L/s]		[µS/cm]		[°C]												[mg/L]										‰ VSMOW		‰ VSMOW		‰ VSMOW		‰ PDB	
			April		April		April		April		April		April		April		April		April		April		April		April		April		April		April		April	
N1	Snow	2,828	-		21		4.3		6.5		0.58		1.1		0.4		4.3		0.4		5.0		1.8		1.0		6.4		-104		-14.5		12.5		-	
N2	Snow	2,812	-		18		4.3		6.5		0.40		0.9		0.1		3.7		0.4		3.6		1.6		0.7		5.4		-92		-13.0		12.3		-	
N3	Snow	2,783	-		36		4.3		6.5		2.14		1.7		1.1		7.2		0.5		15.9		2.7		1.0		7.1		-60		-9.2		13.1		-	
N4	Snow	2,747	-		34		4.3		6.5		1.64		1.3		0.9		7.8		0.4		13.4		2.2		0.9		7.1		-77		-11.2		13.1		-	
N5	Snow	2,703	-		23		4.3		6.5		0.36		0.8		-		6.0		-		6.7		1.5		0.7		6.3		-77		-11.6		16.1		-	
N6	Snow	2,662	-		33		4.3		6.5		0.50		1.0		0.2		12.1		0.2		5.2		2.0		0.7		5.9		-101		-14.3		13.8		-	
N7	Snow	2,636	-		18		4.3		6.5		0.22		0.4		-		4.5		-		3.6		1.3		0.7		5.6		-100		-13.9		11.0		-	
N8	Snow	2,613	-		18		4.3		6.5		0.25		0.3		-		4.7		0.1		3.9		1.2		0.8		5.0		-64		-9.7		13.1		-	
N9	Snow	2,585	-		21		4.3		6.5		0.90		0.5		0.4		4.8		0.2		6.5		1.5		0.8		5.3		-67		-10.0		13.6		-	
N10	Snow	2,585	-		20		4.3		6.5		0.25		0.6		-		3.9		0.4		3.6		1.4		1.3		5.2		-74		-10.8		13.0		-	
N11	Snow	2,513	-		17		4.3		6.5		0.64		0.4		0.2		4.0		0.2		4.7		0.3		0.7		5.0		-52		-7.9		10.8		-	
N12	Snow	2,453	-		17		4.3		6.5		0.53		0.3		0.3		4.0		-		4.4		0.3		1.2		5.0		-86		-12.5		13.9		-	
			J-F	M-J	J-F	M-J	J-F	M-J	J-F	M-J	J-F	M-J	J-F	M-J	J-F	M-J	J-F	M-J	J-F	M-J	J-F	M-J	J-F	M-J	J-F	M-J	J-F	M-J	J-F	M-J	J-F	M-J	J-F	M-J	J-F	M-J
M1	Spring water	2,241	0.10	3.00	31	20	8.4	7.7	6.9	6.4	4.19	0.20	1.8	1.7	0.5	0.3	6.3	5.6	1.7	1.8	28	21	2.0	1.6	1.7	1.5	7.2	7.6	-70	-71	-10.6	-10.7	14.2	14.8	bdl	-14.3
M2	Spring water	2,110	0.10	0.10	54	32	9.3	9.4	7.0	6.9	5.51	0.25	1.3	1.2	0.4	0.5	7.9	7.3	2.1	1.9	36	25	1.8	1.9	1.4	1.5	7.2	6.9	-70	-70	-10.5	-10.5	14.2	13.8	-3.1	-10.7
M3	Spring water	2,107	2.00	10.0	32	19	9.2	9.2	6.6	6.6	5.27	0.40	1.9	1.8	0.5	0.5	6.3	5.6	1.8	1.7	30	24	1.8	1.7	1.4	1.2	7.1	6.9	-71	-72	-10.6	-10.9	13.7	15.2	bdl	bdl
S1	Surface water	2,016	26.8	-	37	15	4.5	6.1	7.9	7.9	0.36	0.49	1.9	0.9	0.2	0.1	7.4	4.8	1.6	0.9	13	9	1.8	1.3	0.9	0.8	11.0	6.4	-74	-72	-11.8	-10.6	20.4	12.8	bdl	bdl
M4	Spring water	2,014	0.20	-	51	45	10.3	10.8	6.9	6.8	5.94	0.33	2.5	2.8	0.4	0.6	8.6	8.3	2.5	2.6	38	30	1.8	1.7	0.7	0.7	13.7	13.4	-71	-71	-10.5	-10.6	13.1	13.8	-6.3	bdl
M5	Spring water	2,012	0.11	-	22	-	10	-	7.0	-	0.52	0.23	2.1	1.3	0.5	0.6	7.7	4.2	1.6	1.3	13	12	2.4	1.7	1.1	1.4	9.9	6.9	-72	-70	-10.9	-10.5	15.5	14.7	bdl	bdl
S2	Surface water	1,998	31.9	51.4	37	17	3.7	11.3	7.8	-	0.32		8.6	-	0.3	-	6.3	-	1.8	-	17	-	2.0	-	0.8		11.3		-74	-	-10.9	-	13.3	-	bdl	bdl
M6	Spring water	1,972	3.00	-	46	33	11.4	10.8	6.9	7.0	5.21	0.41	2.0	2.0	0.5	0.8	8.0	7.2	2.3	2.1	34	28	1.8	2.0	3.2	3.1	9.0	8.1	-70	-70	-10.4	-10.5	13.0	14.0	bdl	-16.5
S3	Surface water	1,822	46.3	-	37	35	4.4	8.5	8.1	7.8	0.27	0.76	3.0	1.9	0.2	0.2	6.6	7.2	1.4	1.6	14	16	1.9	1.5	1.1	0.7	10.6	8.3	-71	-67	-10.8	-9.9	15.4	12.1	bdl	-6.9
P1	Well groundwater	1,810	2.70	-	137	91	11.8	13.6	7.8	8.0	0.03	0.12	6.4	6.7	0.5	0.7	13.5	13.7	4.2	4.3	55	52	1.6	1.8	0.7	0.7	11.5	11.1	-70	-66	-10.7	-10.1	16.0	14.7	-18.3	-18.2
M7	Spring water	1,810	-	3.00	49	41	10.1	10.8	6.9	7.3	5.72	0.42	2.4	1.9	0.4	0.5	7.8	7.7	2.5	2.5	36	23	2.1	1.9	3.0	1.5	10.0	9.1	-69	-69	-10.3	-10.3	13.3	13.7	bdl	-14
P2	Well groundwater	1,647	1.50	-	80	57	13.4	13.7	6.5	6.6	0.02	0.12	3.9	3.6	0.5	0.6	7.5	6.6	3.2	3.3	12	16	3.4	3.3	7.7	7.8	16.6	17.7	-63	-63	-9.5	-9.6	12.9	13.2	bdl	bdl
P3	Well groundwater	1,647	2.50	-	164	51	12.3	12.9	6.3	6.8	0.03	0.09	1.9	1.8	0.7	0.5	10.7	7.2	5.5	3.8	4	21	1.6	2.5	0.7	0.7	46.0	24.2	-69	-70	-10.3	-10.5	13.6	14.4	bdl	bdl

Ref.	Water type	Elevation	Discharge		Elect. Cond.		Temperature		pH		TOC		Na^+		K^+		Ca^{+2}		Mg^{+2}		Alkalinity*		Cl^-		NO_3^-		SO_4^{-2}		δ^2H		$\delta^{18}O$		*d* excess		$\delta^{13}C_{DIC}$	
		[m a.s.l.]	[l·s^{-1}]		[µS·cm^{-1}]		[°C]				[mg·l^{-1}]																		‰ VSMOW		‰ VSMOW		‰ VSMOW		‰ PDB	
			J-F	M-J	J-F	M-J	J-F	M-J	J-F	M-J	J-F	M-J	J-F	M-J	J-F	M-J	J-F	M-J	J-F	M-J	J-F	M-J	J-F	M-J	J-F	M-J	J-F	M-J	J-F	M-J	J-F	M-J	J-F	M-J
M8	Spring water	1,575	0.01	0.50	25	19	10.8	16.2	7.5	6.9	0.01	-	1.4	-	0.4	-	4.8	-	1.3	-	5.5	-	1.7	-	1.6	-	7.2	-	-69	-	-10.5	-	14.4	-	bdl	bdl
M9	Spring water	1,565	<0.01	-	67	-	9.0	-	7.5	-	0.16	-	1.4	-	0.2	-	4.6	-	1.8	-	12.7	-	1.7	-	1.5	-	6.7	-	-69	-	-10.6	-	15.6	-	bdl	bdl
P4	Well groundwater	1,556	2.50	-	32	-	12.0	-	6.5	-	0.19	-	1.6	-	0.3	-	5.2	-	2.1	-	17.2	-	1.7	-	0.9	-	7.8	-	-70	-	-10.7	-	15.8	-	bdl	bdl
M10	Spring water	1,546	-	0.20	66	58	10.3	13.6	7.0	6.8	6.39	0.50	5.2	5.7	0.5	1.0	8.8	8.3	2.9	2.9	50.0	30.0	2.5	2.8	0.8	0.8	14.5	13.2	-62	-61	-9.4	-9.2	13.0	12.6	-4.6	-14.4
M11	Spring water	1,527	-	-	70	63	14.1	14.6	7.6	8.0	5.50	0.55	6.6	7.1	0.3	0.7	8.4	7.8	3.0	3.4	49.8	28.8	2.6	2.6	0.7	0.7	17.8	16.6	-62	-62	-9.4	-9.5	13.4	13.5	-4.0	bdl
M12	Spring water	1,505	1.50	0.01	52	50	9.3	17.7	7.1	7.0	0.75	0.37	3.3	3.6	0.4	0.4	7.6	6.0	2.6	2.7	29.8	21.5	2.7	3.1	4.0	3.5	11.7	11.3	-63	-63	-9.5	-9.3	13.1	11.6	bdl	-12.5
M13	Spring water	1,490	-	0.20	97	86	14.3	14.6	7.0	7.0	5.53	0.38	7.9	8.4	0.5	0.6	10.4	9.8	3.7	3.9	38.0	28.3	2.5	2.4	0.7	0.7	35.9	35.4	-61	-61	-9.3	-9.4	13.0	13.4	-5.6	-14.6
M14	Spring water	1,487	-	-	32	-	12.4	-	6.6	-	0.17	0.34	2.1	1.8	0.3	0.6	7.2	5.1	2.5	2.0	30.1	26.7	2.0	2.0	3.7	1.6	8.1	7.6	-69	-69	-10.3	-10.2	13.5	13.2	bdl	-13.3
M15	Spring water	1,485	-	0.01	97	89	11.8	13.9	6.8	6.5	11.77	0.49	7.4	7.7	0.4	0.7	11.5	10.9	4.4	4.3	54.7	52.8	3.2	3.1	0.8	0.8	26.4	23.5	-62	-62	-9.2	-9.4	12.1	13.3	-7.4	-15.7
M16	Spring water	1,460	-	1.36	41	40	11.2	13.2	6.5	6.3	0.21	-	2.2	-	0.3	-	6.9	-	2.6	-	28.0	-	2.0	-	3.1	-	9.1	-	-67	-	-10.1	-	13.3	-	bdl	bdl
M17	Spring water	1,451	-	6.50	40	30	12.9	13.7	6.4	6.3	0.30	0.28	1.9	2.0	0.4	0.2	6.8	5.6	2.3	2.6	28.1	26.9	1.9	2.4	1.8	2.5	7.7	8.4	-68	-68	-10.2	-10.2	13.5	13.2	bdl	-16.7
S4	Surface water	1,441	83.6	80.7	58	26	5.7	11.0	8.0	-	0.33	0.45	2.2	3.7	0.4	0.2	7.9	9.0	2.2	3.1	22.0	25.9	2.5	1.9	0.7	0.7	14.6	10.8	-68	-68	-10.2	-10.1	13.5	12.8	-2.8	-4.3
S5	Surface water	1,438	36.5	-	37	-	5.1	-	8.0	-	0.07	0.71	1.6	0.4	0.2	0.2	4.8	3.5	1.7	0.8	7.7	19.5	1.9	1.6	1.9	0.7	6.4	8.5	-71	-70	-10.6	-10.5	13.9	13.6	bdl	bdl
M18	Spring water	1,331	0.34	0.63	112	111	15.1	14.6	7.5	7.2	0.24	0.46	4.6	5.1	1.8	2.1	14.3	14.7	4.1	4.1	51.0	28.6	4.3	4.5	10.2	10.0	23.6	23.0	-67	-68	-10.1	-10.3	13.1	14.3	-5.1	-14.3
M19	Spring water	1,328	0.15	0.35	109	126	13.0	13.3	6.8	6.6	0.27	0.42	3.4	3.7	0.8	1.1	15.6	17.5	5.2	6.0	57.9	46.7	3.1	3.0	12.1	14.5	26.2	24.7	-67	-67	-10.0	-10.2	12.7	14.2	-3.9	-14.9
M20	Spring water	1,320	0.11	0.58	116	90	15.3	14.2	7.7	6.8	0.21	0.43	2.7	3.1	0.7	0.6	10.3	11.6	3.9	4.9	38.0	30.4	2.4	3.2	6.9	10.8	17.4	16.2	-67	-67	-10.0	-10.0	12.9	12.8	-8.7	-16.1
M21	Spring water	1,313	0.05	0.10	61	75	13.2	15.2	7.9	8.0	0.21	0.40	2.8	3.1	0.2	2.7	11.7	11.3	3.1	3.4	46.0	28.4	2.6	4.9	4.5	6.3	11.1	12.0	-64	-65	-9.5	-9.6	12.1	11.8	-7.5	bdl
M22	Spring water	1,296	0.03	0.13	55	55	14.3	14.1	7.0	7.1	0.25	0.29	3.0	3.2	0.4	0.4	8.1	6.8	3.3	3.3	35.8	26.0	2.3	2.8	5.3	3.1	12.0	11.1	-68	-68	-10.1	-10.3	12.8	14.2	-7.6	-14.7
M23	Spring water	1,288	0.13	0.26	58	59	13.4	15.1	8.0	7.2	0.47	0.32	2.8	3.5	0.4	0.6	8.9	8.9	3.4	3.6	38.0	23.2	2.4	3.0	3.7	4.3	12.2	12.7	-67	-68	-10.1	-10.2	13.7	13.6	-6.0	-13.2
G1	Spring water	1,261	0.14	0.22	100	101	13.3	15.9	7.4	7.3	0.29	0.50	3.6	6.8	0.7	0.4	13.5	11.3	5.0	4.9	62.9	38.1	3.2	4.8	3.0	2.3	28.9	25.0	-63	-63	-9.4	-9.6	11.7	13.6	-5.0	-11.1
G2	Spring water	1,252	0.38	0.85	158	149	15.3	15.6	7.1	7.2	0.24	0.80	6.7	7.4	1.3	1.4	18.0	19.8	5.9	6.4	82.8	68.7	4.2	5.0	8.9	8.5	34.8	33.7	-64	-64	-9.7	-9.7	13.5	13.6	-5.2	-14.1
G3	Spring water	1,214	0.08	0.30	243	231	14.8	14.6	7.3	7.4	0.45	0.60	10.1	9.6	2.5	2.7	34.2	33.6	8.3	7.7	146.8	76.1	7.8	6.7	10.0	7.7	66.3	55.1	-64	-64	-9.7	-9.4	13.8	11.9	-5.8	-14.3
S6	Surface water	1,202	149	-	75	-	6.5	-	7.6	-	0.37	-	5.4	-	0.4	-	14.0	-	4.6	-	27.6	-	2.7	-	0.9	-	18.1	-	-67	-	-10.3	-	14.7	-	-1.9	bdl
S7	Surface water	1,190	14.9	-	100	80	5.9	13.3	7.4	7.6	0.27	0.68	4.7	4.3	0.4	0.4	12.0	11.1	4.2	4.1	41.7	35.1	2.8	3.0	0.8	1.0	19.7	14.9	-69	-65	-10.5	-9.8	15.2	13.1	-0.2	-4.2
G4	Spring water	1,176	0.06	0.08	1,132	1188	15.7	15.5	6.1	6.2	0.05	0.25	104.8	105.5	8.2	8.7	30.6	114.1	44.9	43.1	834.6	1,102	32.9	33.4	0.7	0.7	84.6	83.8	-	-65	-	-9.8	-	13.7	1.4	-1.4
S8	Surface water	996	-	-	114	114	6.9	13.4	8.1	8.0	0.48	0.71	6.5	5.6	0.5	1.1	18.1	19.1	6.4	5.4	49.3	53.8	3.3	3.0	0.9	0.9	26.0	20.8	-70	-67	-11.3	-10.0	20.2	13.3	-3.5	-7.4

(continuation of Table 1)

Water mineralization apparently increases as altitude decreases (Fig. 6A), in both surface water and groundwater. Between 2250 and 1250 m a.s.l. the ∇_zEC is -10 µS/cm/100 m. This occurs for the whole set of water samples, except for the most chemically evolved groundwater (wells P1 and P3 and springs M18, M19, M25, M26 and G), which outflows at a relatively similar elevation (1200-1300 m a.s.l. and 1700-1800 m a.s.l., for wells and springs respectively) yet shows EC values ranging up to one order of magnitude (Table 1 and Figure 6A). No substantial differences in the degree of mineralization are observed between the two sampling campaigns for most water types, except for wells P1 and P3.

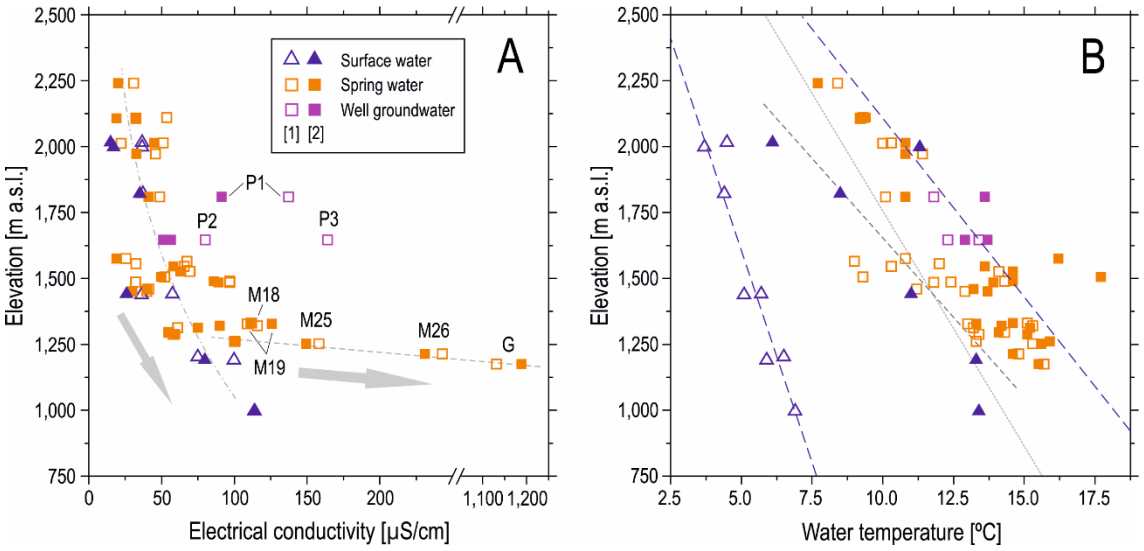

Figure 6: Altitudinal variation of electrical conductivity (A) and water temperature (B) of surface waters and groundwater collected in the BRW. Numbers in brackets refer to the field surveys of January-February [1] (open symbols) and May-June [2] (solid symbols).

In the BRW, the atmospheric mean temperature vertical gradient ($\nabla_z T_{atm}$) is -0.62 ºC/100 m (Fig. 6B). According to temperature data in surface waters, the computed temperature

vertical gradient ($\nabla_z T_{sw}$) was -0.27 ºC/100 m for the first field survey (January-February 2015) and -0.53 ºC/100 m for the second one (May-June 2015). As seen, $\nabla_z T_{sw}$ is closer to $\nabla_z T_{atm}$ in the later field campaign. In the case of groundwater, $\nabla_z T_{gw}$ is similar to $\nabla_z T_{atm}$ regardless of the sampling season (Fig. 6B).

4.3 H, O and C stable isotopes

Snow samples display the widest range of variation for stable water isotopes, ranging from -52‰ to -104‰ for δ^2H, and from -7.9‰ to -14.5‰ for δ^{18}O (Table 1 and Fig. 7A). Surface water and groundwater samples have, overall, similar signatures and cluster in a reduced isotopic interval: -60‰ to -75‰ for δ^2H, and -9‰ to -12‰ for δ^{18}O.

In Figure 7 the data set is plotted jointly with the Global Meteoric Water Line (GMWL, Craig, 1961) of slope 8 and deuterium excess *d* = 10‰. For comparison, the parallel lines of *d* = 13‰ and *d* = 14‰ are also included, the latter representing the western Mediterranean average line.

The April snow water samples adapt well to *d* = 13‰ irrespective of the altitude, and cover a wide range of values representing precipitation. Surface water has a lower and isotopically lighter range and winter waters tend to be different from springtime waters, with some overlapping. While May-June samples adapt to the April snow line, yet with a smaller range, January-February samples are the lightest and tend to have higher to much higher deuterium excess, up to 20‰. The highest values could be suspected of analytical error; but they are probably not, as other samples likewise show a trend to high deuterium excess. This cannot be explained without a time series of precipitation isotopic data. It may, however, be the result of condensed atmospheric water vapor enriched by continental water evaporation along the wind path from the Atlantic Ocean, and produced in a relatively dry atmosphere.

346 Spring and well water samples plot around the LMWL (*d* = 13‰; Figure 7) with some
347 deviations that clearly do not depend on the sampling campaign: a) the lightest ones tend
348 to shift to higher *d* (WMWL) as winter surface waters; b) the isotopically heaviest waters
349 tend to move to lower *d* (GMWL) that may be caused by a slight evaporation effect during
350 recharge. The latter isotopic signature can be expected since they correspond to the lowest
351 altitudes. In fact, some May-June surface water samples also show a possible slight
352 evaporation effect, pointing to water seasonality and the need for repeated sampling to
353 better understand the hydrological processes.

354 Two clusters of spring and well waters can be distinguished (Fig. 7): 1) an isotopically
355 lighter group from the upland catchment and a heavier group located in the vicinity of the
356 *acequias de careo* and irrigation canals but that also includes groundwater samples from
357 springs and wells that are not influenced by the *acequias de careo* recharge; and 2) spring
358 G$_2$ which discharges iron-rich groundwater.

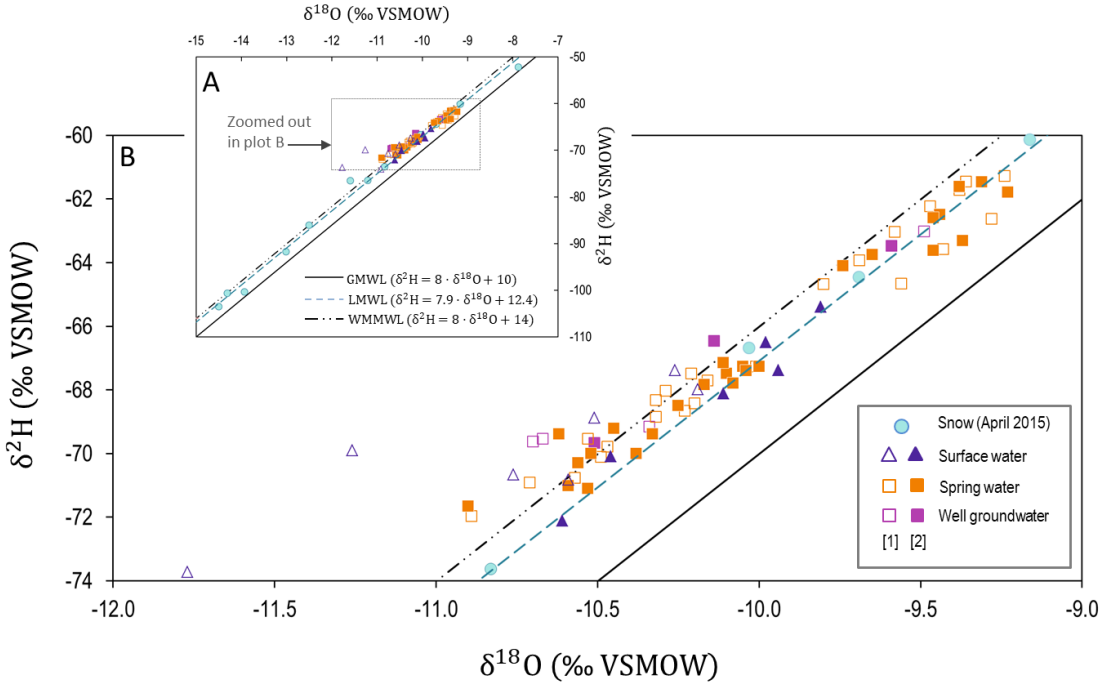

359

Figure 7: δ^2H *vs* $\delta^{18}O$ plot for all water samples (A) and for surface waters and groundwater (B) from the BRW. In the legend, [1] (open symbols) and [2] (solid symbols) refer to the winter (January-February) and spring (May-June) sampling campaigns. GMWL (d = 10‰), LMWL (d = 13‰) and WMMWL (d = 14‰) stand for Global, Local and Western Mediterranean Meteoric Water Line, respectively.

Waters from the BRW show variable $\delta^{13}C_{TDIC}$ (1.4 ‰ to -18.3 ‰) and low alkalinity values, mostly below 90 mg/L (Table 1). In fact, 38% of the analyzed water samples had insufficient concentrations of dissolved inorganic carbon (DIC) to ensure reliable $\delta^{13}C_{TDIC}$ determinations. Figure 8A is a plot of $\delta^{13}C_{TDIC}$ versus HCO_3. It is considered that current atmospheric CO_2 has $\delta^{13}C_{TDIC}$ ~ -7‰ and biogenic soil CO_2 is about -23 to -25‰ $\delta^{13}C$. Incorporation of CO_2 into water is assumed to mostly takes place in an open system at a pH (Fig. 8B) in which HCO_3 dominates, so at the ambient temperatures there is an isotopic fractionation of ~ -8‰. It is also assumed that there are no carbonates in the soil. Surface water is isotopically heavy, reflecting the dominance of atmospheric CO_2 in the winter samples (the heaviest) and a mixture of soil and atmospheric CO_2 in spring or atmospheric CO_2 dissolution under acidic pH (not so heavy). Spring waters cluster in two non-overlapping groups, the heaviest for winter samples, around -5‰, and the lightest for springtime samples, around -14‰. The latter value corresponds to biogenic soil CO_2 and the former one to a mixed situation. In any case there is a no great increase of HCO_3 (with one exception), meaning that rock weathering is undergone at the earlier stages. The only well water with $\delta^{13}C$ determination shows no seasonal difference and the possible effect of biogenic soil CO_2 under a lower *in situ* pH.

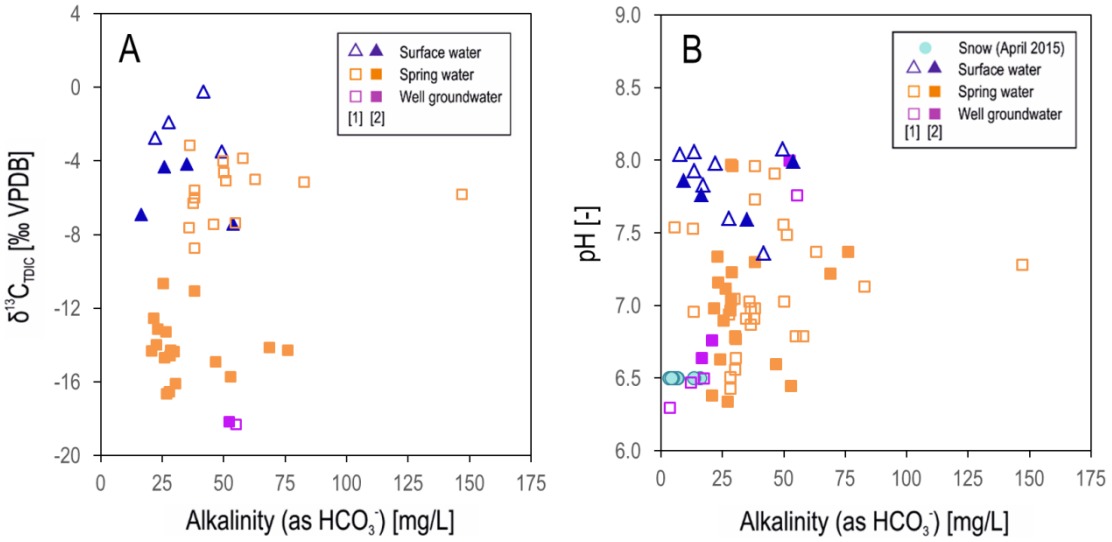

383

384 **Figure 8:** (A) Relationship between $\delta^{13}C_{TDIC}$ and alkalinity (as HCO_3^-). Note that not all
385 water samples are represented due to the generally low concentration of dissolved
386 inorganic carbon. DIC from soil assumes isotopic equilibrium in an open to CO_2 system;
387 (B) Relationship between pH and alkalinity. In the legend, [1] (open symbols) and [2]
388 (solid symbols) refer to the winter (January-February) and spring (May-June) sampling
389 campaigns.

390

391 **5. Data interpretation and discussion**

392 5.1 Preliminary evaluation of aquifer recharge using the chloride mass balance method
393 (CMB)

394 Environmental tracers are a well-known tool for estimating long-term average rainfall
395 diffuse recharge to aquifers (Eriksson, 1960; Eriksson and Khunakasen, 1969; Custodio
396 and Llamas, 1976/1983; Wood and Sanford, 1995; Wood, 1999; Alcalá and Custodio
397 2014; 2015; Custodio and Jódar, 2016; Custodio et al., 2018; among others). The
398 atmospheric CMB method (Claasen et al., 1986; Dettinger, 1989; Sami and Hughes,
399 1996; Scanlon et al., 2006; Custodio, 2010; Alcalá and Custodio, 2014; and references

400 therein) takes advantage of the almost conservative behavior of the chloride ion (Cl^-).
401 Rainwater incorporates atmospheric chloride bulk deposition in the hydrological system.
402 One part flows dissolved with surface runoff and other part percolates through the vadose
403 zone. As a result of the evapotranspiration process in the soil root zone, dissolved chloride
404 concentrates and, therefore, the solute concentration of recharge rises with respect to that
405 in rainwater, as can be seen in Figure 9.

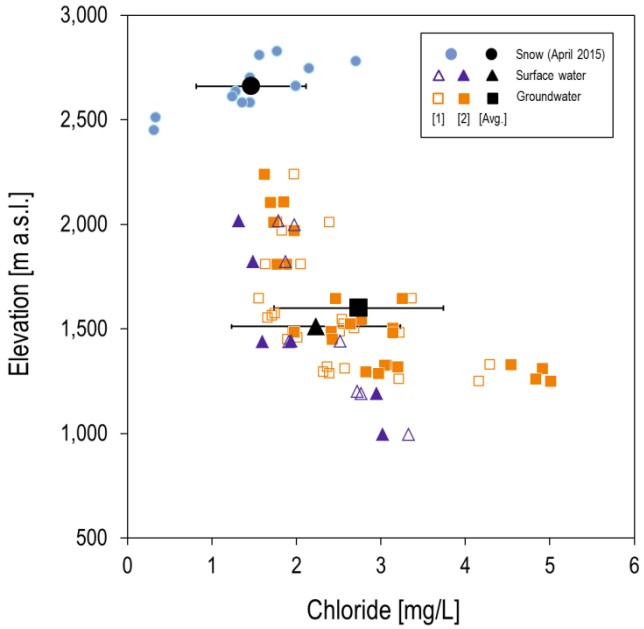

406

407 **Figure 9:** (A) Altitudinal variation of chloride content in snow (circles), surface water
408 (triangles) and groundwater (squares) collected in the BRW. Numbers in brackets indicate
409 field surveys of January-February [1] and May-June [2]. Black symbols indicate the
410 average value and the error bars show the corresponding standard deviation.

411

412 Given a long enough period in a natural gradient hydrological system in which the long-
413 term storage variations of chloride in both soil and vadose zones can be assumed to be
414 negligible, the steady state chloride mass balance equation can be described by

$$C_T q_T = C_{gw} q_{gw} + C_{sw} q_{sw} \quad (1)$$

where q [LT^{-1}] and C [ML^{-3}] are water runoff and chloride concentration, respectively, and the subscripts "*T*", "*groundwater*" and "*sw*" stand for the total basin discharge, groundwater discharge and surface runoff, respectively. The values of q_T (195 mm/year, Jódar et al., 2017) and C_T (3.2 mg/L) are obtained from averaging the measured basin discharge and the chloride concentration (S8, Table 1), respectively, at the Narila gauging station (S8, Fig. 1). The value of C_{gw} (2.7 mg/L) can be approximated by the average chloride content measured in groundwater samples (i.e. springs and wells, Table 1). The variables q_{gw}, q_{sw} and C_{sw} are unknown. Nevertheless, the last term of Equation 1 can be expressed as

$$A_E = C_{sw} q_{sw} \quad (2)$$

where A_E [$ML^{-2}T^{-1}$] is direct surface runoff chloride mass flux. Alcalá and Custodio (2014) provide mean annual values of this variable ($\overline{A_E}$) for the whole continental Spain. Including A_E into Equation 1 allows estimating groundwater discharge as

$$q_{gw} = \frac{C_T q_T - A_E}{C_{gw}} \quad (3)$$

In the case of the BRW, $\overline{A_E}$ varies between 0.1 and 0.25 g/m^2/year (Fig. 10A, Table 2), whereas q_{gw} ranges between 190 and 135 mm/year, respectively corresponding to 97% and 69% of the total basin discharge. These high values are consistent with those obtained by Al-Awani (1997) and Jódar et al. (2017, 2018). Taking into account that the BRW presents areas of high slope with presumably low-permeability hard rock substrate, the obtained high groundwater contribution to the total basin discharge underlines the role

played by the recharge canals in the hydrological response of the basin. Moreover, the fast transition from the altered rock zone to the fresh metamorphic bedrock zone makes regional deep flows play a minor role from a discharge perspective. Along this line and from a steady state hydrological point of view, aquifer recharge may be approximated to q_{gw}. Therefore, taking into account the obtained groundwater discharge variation interval, recharge can be assumed to represent 16% to 22% of the mean annual precipitation in the BRW, which is 828 mm/year.

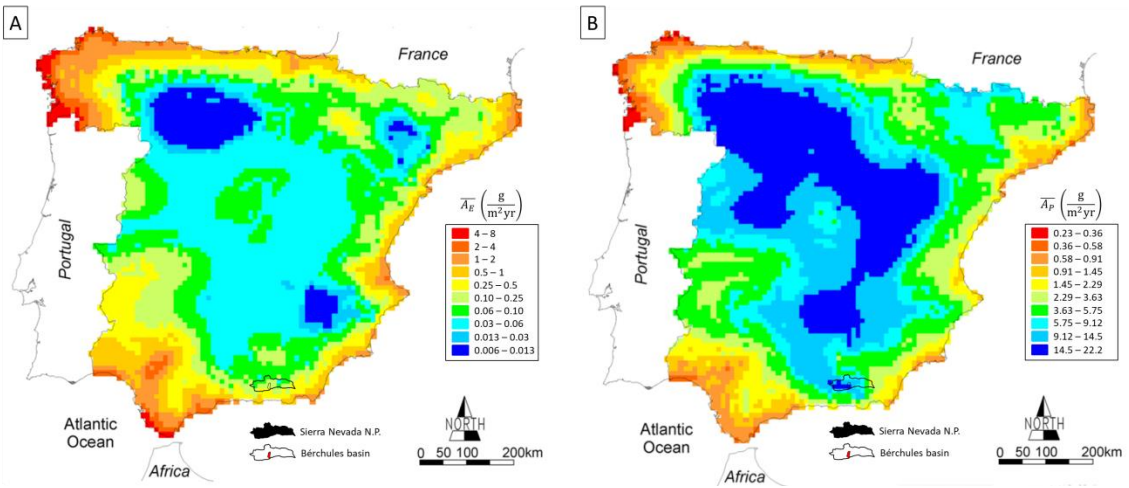

Figure 10: Mean annual chloride mass flux by direct surface runoff $\overline{A_E}$ (A) and for atmospheric bulk deposition $\overline{A_P}$ (B), in continental Spain (modified from Alcalá and Custodio, 2014).

5.2 Mechanisms for mineralization of groundwater

In all the sampled points, except spring G, groundwater presents a low mineralization that can be explained by evaporitic concentration of dissolved salts in precipitation. This is reflected by Cl and also SO_4 concentrations. The other ions —except HCO_3, which partly depends on equilibrium with air CO_2— show higher concentrations, pointing to other

mineralization processes in the soil, namely the weathering of rock and soil minerals. These processes affect the groundwater hydrochemical composition in two different ways (Fig. 6A). On the one hand, most groundwater is quickly drained through springs (and likely intercepted by pumping wells) in the uplands and intermediate altitude catchment, with EC values ranging from 20 to ~150 µS/cm. On the other hand, several groundwater samples from springs and wells in the lowlands that show higher water mineralization are associated with local drainage of groundwater polluted by urban wastewaters and with springs draining major deep fractures (i.e. site G). The preferential quick flows through weakly soluble silicate rocks forming the shallower layer of the crystalline aquifer (i.e. weathered zone) result in low solute content spring waters. Groundwater discharge from some low yield springs located downflow from the urbanized area in Alcútar, a small village just 1 km northwest of the Narila gauging station, is highly mineralized, indicating wastewater influence.

The temperature of surface waters in the BRW fits to some extent the estimated altitudinal gradient of the mean air temperature (-0.62 ºC/100 m; Fig. 6B). The vertical thermal gradient obtained from measurements in surface waters ($\nabla_z T_{sw}$) reflects a thermal disequilibrium in this water along the river course. In May-June, the variation along elevation of $\nabla_z T_{sw}$ is due to snow melt in the river stretch through the snow and ice caps. The air-water thermal equilibrium is also perceptible in most groundwater samples, since the main flow routes promoting fast flows are found in shallow subsurface (through the weathered zone of the metamorphic bedrock, no deeper than 50-60 m below land surface), very often following pathways parallel to the uneven land surface.

5.3. Estimation of recharge rate

Infiltrating water incorporates dissolved salts as solutes in groundwater. Soil-water evaporation and plant transpiration enhance the dissolved salts concentration in infiltrating water as a consequence of the water-mass reduction they produce. Assuming that chloride behaves as a conservative tracer, it is possible to estimate the mean chloride content in the evaporated precipitation $\overline{C_R}$ [ML^{-3}] as (Alcalá and Custodio, 2014):

$$\overline{C_R} = \frac{1}{\bar{R}}(\overline{A_P} - \overline{A_E}) \quad (4)$$

where $\bar{R}$ [ML^{-3}] is the mean annual recharge and $\overline{A_P}$ [$ML^{-2}T^{-1}$] is the atmospheric bulk deposition of chloride (Fig. 10B). Once $\overline{C_R}$ is obtained, the evaporation concentration factor ξ [-] can be obtained as

$$\xi = \frac{\overline{C_R}}{\overline{C_P}} \quad (5)$$

where $\overline{C_P}$ [ML^{-3}] is the average chloride content in precipitation. This variable can be estimated in terms of the mean annual precipitation $\bar{P}$ [LT^{-1}] and $\overline{A_P}$, provided that $\overline{A_P} = \overline{C_P} \cdot \bar{P}$ (Alcalá and Custodio, 2014). Table 2 gives the variation interval of $\bar{R}$, $\overline{A_E}$, $\overline{A_P}$, $\overline{C_P}$ and $\overline{C_R}$ in the BRW. Taking into account these values, a variation interval for ξ between 3 and 7.7 is obtained. This concentration interval is considered valid for the other dissolved salts in precipitation. Figure 11 offers a Schöeller-Berkaloff diagram showing the major ion concentrations in the evaporated recharge. To obtain these values it is assumed that the chemical composition of precipitation corresponds to the average composition of all the snow samples taken in the BRW during April 2015. The observed concentrations of Na, Ca, Cl and SO_4 in groundwater can be explained by only considering the process of precipitation concentration by evaporation. The contents of Mg and HCO_3 in groundwater are higher than those for the evaporated precipitation. As

494 shown in the next section, these increments can be traced to chemical interaction between
495 the recharge water and the minerals of the geological formation.

496

497 **Table 2.** Variation interval values for mean annual values of precipitation ($\bar{P}$), direct
498 surface runoff chloride mass flux ($\overline{A_E}$), atmospheric bulk deposition of chloride ($\overline{A_P}$),
499 mean chloride content in both precipitation ($\overline{C_P}$) and recharge ($\overline{C_R}$.), and evaporation
500 concentration factor (ξ) in the BRW.

	$\bar{R}$ (mm/yr)	$\overline{A_E}$ (g/m^2/yr)	$\overline{A_P}$ (g/m^2/yr)	$\overline{C_P}$ (mg/L)	$\overline{C_R}$ (mg/L)	ξ **(-)**
Min	135	0.10	12.70	15.34	45.56	2.97
Max	190	0.25	19.63	23.71	181.44	7.65

501

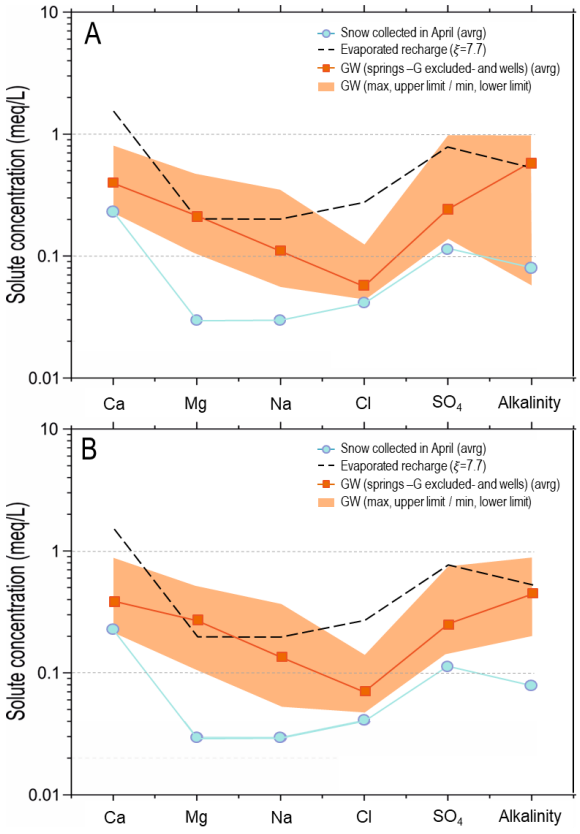

502

503 **Figure 11.** Schoeller-Barkaloff diagram of the mean compositions of precipitation (i.e.
504 snow), evaporated recharge and groundwater in the BRW. (A) January-February
505 sampling campaign and (B) May-June sampling campaign.

506

507 5.4 Water-rock chemical interactions

508 Based on field observations, the lithology found at the test site, the plausible mineralogy
509 and the analytic results derived from this study, the following reactions are the most
510 probable, assuming final pH is in the range where HCO_3 is the dominant inorganic
511 dissolved carbon species:

512 Albite hydrolysis,

$$2NaAlSi_3O_8 + 2CO_2 + 1H_2O \rightarrow Al_2Si_2O_5(OH)_4 + 2HCO_3^- + 2Na^+ + 4H_4SiO_4 \quad (6)$$

513 K-feldspar hydrolysis,

$$2KAlSi_3O_8 + 2CO_2 + 6H_2O \rightarrow Al_2Si_4O_{10}(OH)_2 + 2HCO_3^- + 2K^+ + 4H_4SiO_4 \quad (7)$$

514 Anorthite hydrolysis (congruent),

$$CaAl_2Si_2O_8 + 2CO_2 + 3H_2O \rightarrow Al_2Si_2O_5(OH)_4 + 2HCO_3^- + Ca^{+2} \quad (8)$$

515 Tremolite hydrolysis (congruent),

$$\begin{aligned} Ca_2Mg_5Si_8O_{22}(OH)_2 + 14CO_2 + 22H_2O \\ \rightarrow 2Ca^{+2} + 5Mg^{+2} + 8H_4SiO_4 + 14HCO_3^- \end{aligned} \quad (9)$$

516 Calcite dissolution,

$$CaCO_3 + CO_2 + H_2O \rightarrow Ca^{+2} + 2HCO_3^- \quad (10)$$

517 Dolomite dissolution (congruent),

$$2CO_2 + 2H_2O + CaMg(CO_3)_2 \leftrightarrow Ca^{+2} + Mg^{+2} + 4HCO_3^- \quad (11)$$

518

519 In the case of dominantly acidic water not related to CO_2 dissolution, the above reactions
520 can be rewritten by placing one H^+ in the left hand side for every HCO_3 in the right hand
521 side and deleting CO_2 (left hand side) and HCO_3 (right hand side).

522 Most of the water samples collected in the BRW (except for snow water samples, Fig.
523 12A) show a marked chemical gradient between Na-rich compositions; this would be the
524 result of hydrolysis processes of silicate minerals (e.g. albite), and Ca-Mg water types
525 representing reaction products from the dissolution of minerals enriched in such divalent
526 cations (e.g. anorthite, garnet and amphibolite). According to the anorthite hydrolysis
527 reaction (Eq. 8, Fig. 12B), a general calcium excess is observed in the majority of surface
528 water and groundwater, which appears to be greater for the sample cluster corresponding
529 to the January-February field survey.

530 Regarding the relationship between Mg and alkalinity (Fig. 12C), Mg-rich silicate
531 minerals, as amphibolite (mainly tremolite), and the horizons of dolomite, may contribute
532 to the magnesium excess, with stoichiometric ratios of 5:14 and 1:4, respectively. This is
533 the case of neutral or moderately basic water, but not for carbon dioxide related acidic
534 water, where the ratio can be much higher, depending on original acidity.

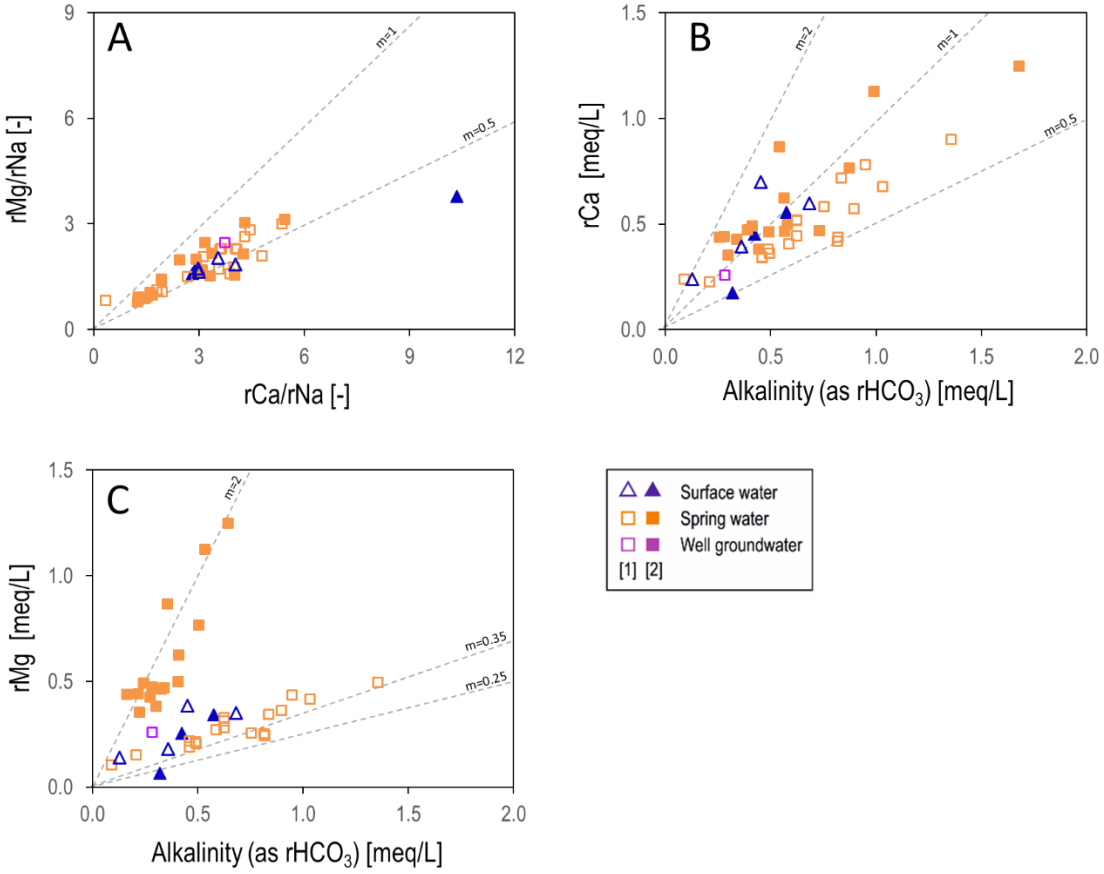

535

536 **Figure 12:** Relationships between (A) the ratios rMg/rNa and rCa/rNa, (B) rCa and
537 alkalinity, and (C) rMg and alkalinity (r means the concentrations are expressed in
538 meq/L). The dashed lines indicate constant slope (m) ratios.

539

540 The most abundant anions in surface waters and groundwater sampled in the BRW are
541 HCO_3 and SO_4, while the dominant cations correspond to Ca and Mg (Table 1 and Fig.
542 5). As carbonate formations are not present in the metamorphic basement, HCO_3 and
543 divalent cations have a common origin in the chemical weathering of silicate minerals
544 and the dissolution of air CO_2 in the soil-weathered shallow zone of the aquifer, or directly
545 from the atmosphere in the case of direct surface runoff or snowmelt. The dissolved
546 inorganic carbon is assumed to come from biogenic CO_2 in soil air and atmospheric CO_2,
547 as explained before.

548 The excess of cations not directly related with HCO_3 increase, even considering that part
549 of Ca is precipitated (incongruent dissolution), possibly due to acidic rain. This has not
550 been considered in the study.

551

552 5.5 Evidence of diffuse groundwater pollution

553 Dissolved NO_3 in sampled waters shows two distinctive evolutions in the BRW (Figs.
554 13A and 14). On the one hand, a subtle enrichment in NO_3 (of 0.05 meq/L or 2.4 mg/L
555 as much) is detected in both surface waters and spring waters as the elevation
556 progressively diminishes, from the top to the lower parts of the watershed. On the other
557 hand, in the ranges of elevation 1200-1400 m a.s.l. and 1800-2200 m a.s.l. (coinciding
558 with the irrigated areas in high- and low-lands), the NO_3 contents measured in
559 groundwater become highly variable, reaching a maximum close to 0.25 meq/L (12 mg/L
560 NO_3) (Fig. 13A). This occurs regardless of the season.

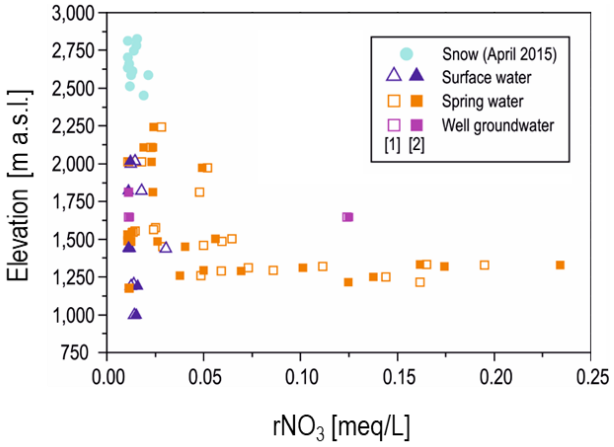

561

562 **Figure 13:** Relationships between elevation and rNO_3 (r means the concentrations are
563 expressed in meq/L). In the legend, [1] and [2] refer to the winter (January-February) and
564 spring (May-June) sampling surveys.

565

566 5.6 Factors influencing the isotopic signature of groundwater

567 There is a relationship between elevation and the isotopic composition of spring waters
568 that are not affected by the *acequias de careo* recharge system (Fig. 14). These springs
569 include the ones located above the recharge canals (M1 to M7) in the upper part of the
570 basin and those located in the lower part of the basin where such recharge canals are not
571 present (M11-M13, M15, M21, M24-M26 and G). For all those springs, the vertical
572 gradients of isotopic content in groundwater ($\nabla_z \delta^{18}O_{GROUNDWATER}$) in winter and spring
573 are -0.13‰/100 m and -0.14‰/100 m, respectively. These values are both lower than the
574 -0.17‰/100 m vertical gradient of isotopic content in precipitation ($\nabla_z \delta^{18}O_P$) (Fig. 14).
575 This result indicates that in the zones where the *acequias de careo* recharge the
576 hydrogeological system, it behaves as a sloping aquifer (Custodio and Jódar, 2016) where
577 rainfall recharges the aquifer along the mountain slope. This interpretation agrees with
578 the presence of Quaternary deposits (glacial, alluvial, soil sliding, peri-glacial debris and
579 alluvial fan sediments; Fig. 1) along with highly fractured metamorphic materials that
580 form the upper part of the aquifer.

581 The isotopic composition of the springs affected by the *acequias de careo* recharge (M8,
582 M9, M10, M14, and M16 to M23) does not show any relationship with elevation. These
583 springs are characterized by an isotopic composition that corresponds to that of a higher
584 elevation zone, comprised between 2000 and 2800 m a.s.l. The upper elevation limit is
585 higher in winter than in spring (Fig. 14). The isotopic fingerprint of the *acequias de careo*
586 recharge water is defined by the isotopic composition of the surface water sampled in S1
587 (Fig. 1). This is the point where the melt water flowing from the higher part of the Chico
588 river basin is derived into the canal network.

589 The surface water sampling point S3 drains the upper part of the Grande River. This melt
590 water tributary zone has a lower elevation than that corresponding to sampling point S1.
591 Hence, the isotopic composition measured in S3 is heavier than that measured in S1 (Fig.
592 14). Melt water flowing through S3 is derived into the Las Hoyas irrigation canal that
593 recharges the aquifer in the lower part of the basin, which is likewise drained by the
594 Bérchules River.

595

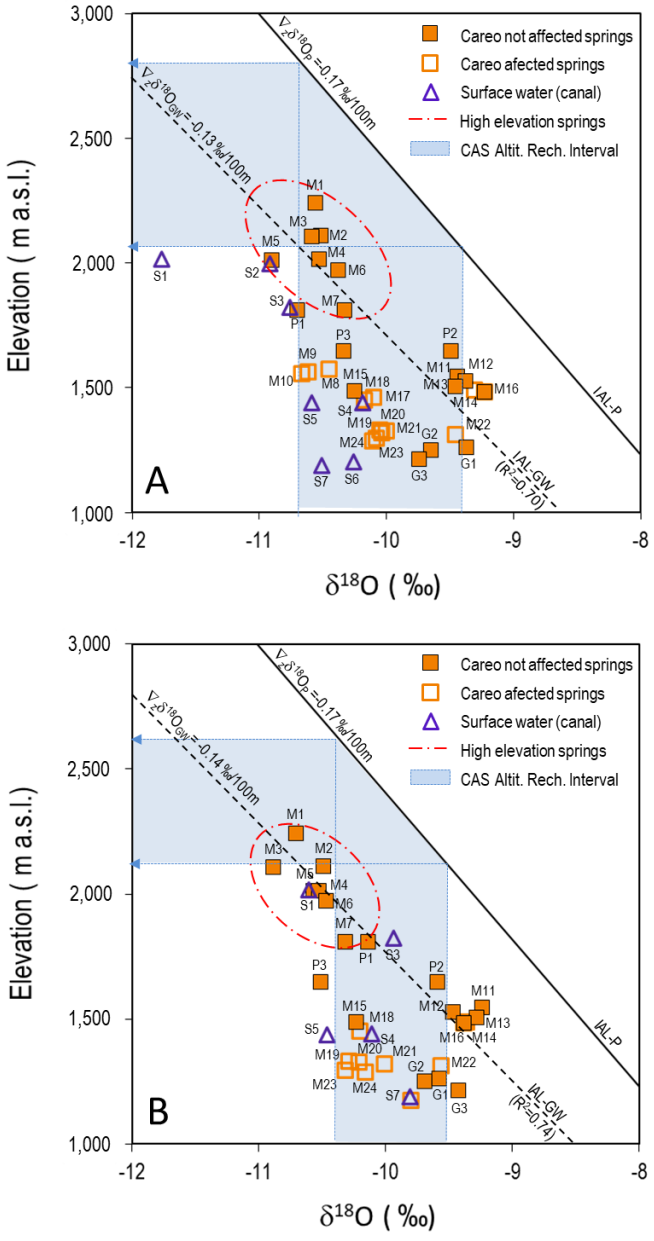

596

597 **Figure 14:** Relationship between $\delta^{18}O$ and elevation for groundwater (squares) and
598 surface water (triangles) in the sampling campaigns of winter (A) and spring (B) seasons.
599 Solid symbols stand for springs not affected by the recharge through *acequias de careo*.
600 IAL-P is the isotopic altitudinal line obtained with data from this study and published
601 rainfall isotopic data from Raya Garrido (2003), Fernandez-Chacón et al. (2010) and
602 Jiménez-Gavilán (2010). IAL-GW-1 is the isotopic altitudinal line obtained for
603 groundwater using the isotopic content data from the sampled springs not affected by the
604 upstream recharge through the *acequias de careo* system. The light-blue shaded area
605 indicates the recharge elevation interval corresponding those springs not affected by the
606 *acequias de careo* recharge system. The interval is obtained by projecting the minimum
607 and maximum $\delta^{18}O_{GROUNDWATER}$ values on the IAL-P.

608

609 5.7 Conceptualization of the groundwater flow system

610 The results derived from the analysis of the hydrogeologic, hydrogeochemical and
611 isotopic data collected in the BRW outline the existence of two clearly differentiated
612 groundwater flow types. The main type includes low-mineralized groundwater (15-164
613 µS/cm), with calcium-magnesium bicarbonate-sulphate chemical facies and pH values
614 around 7 (Table 1 and Figs. 5 and 6). This groundwater flow system drains a mixed
615 granular-hard rock aquifer that developed over the weathered zone of the Palaeozoic
616 schists cropping out in the study area (Figs. 1 and 15). In a secondary flow path, solute-
617 enriched groundwater (EC > 1100 µS/cm and pH ~ 6) flows across the BRW through the
618 deep master fracture network hosted in the metamorphic bedrock (Fig. 15). In this study,
619 this groundwater type is represented only by the G spring water (Figs. 1, 5). Nevertheless,

its occurrence along the southern edge of Sierra Nevada is frequent in similar hydrogeologic settings (Castillo and Fedeli, 2002).

The main hydrogeological system is relatively shallow (average thickness < 50 m) and the predominant low-mineralized groundwater flow system is mainly controlled by the slope configuration of the metamorphic basement (Fig. 15). The similar values observed for $\nabla_z T_{atm}$ and $\nabla_z T_{gw}$ reflect the existence of a shallow aquifer in which groundwater predominantly flows close to the soil surface. The most mineralized groundwater samples correspond to springs associated with regional fractures affecting the metamorphic bedrock. Regarding the isotopic content in groundwater, the springs located in the upper part of the basin discharge an isotopically lighter groundwater; conversely, the springs located at lower elevations discharge an isotopically heavier groundwater (Table 1 and Fig. 1). Thus, there is an altitudinal isotopic gradient lower than that defined by the meteoric waters (Fig. 14). Such an isotopic anomaly is coherent with a sloping aquifer situation (Custodio and Jódar, 2016), by which runoff infiltration in the BRW is produced following the major axis of the river basin, where the sediments of the weathered zone have preferentially accumulated.

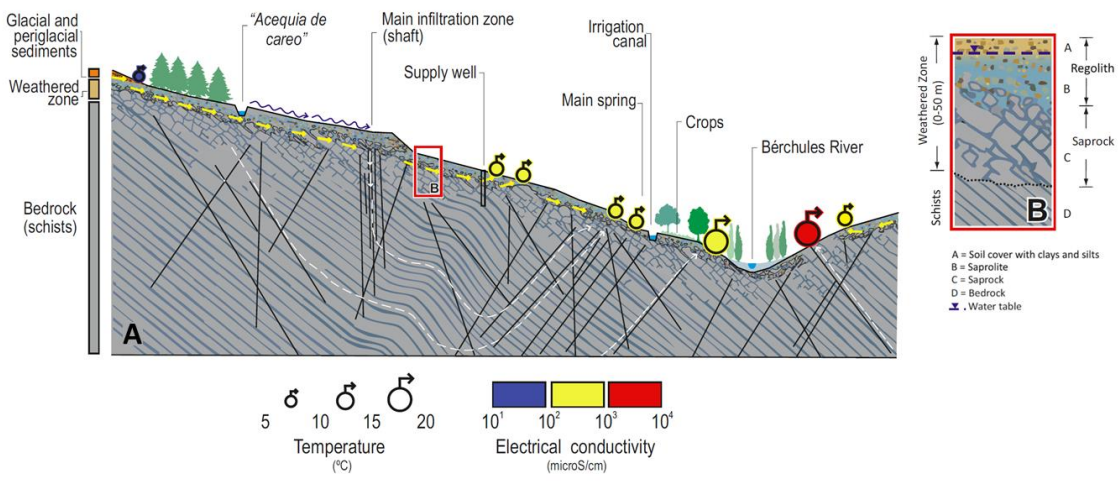

Figure 15: (A) Idealized scheme of groundwater flow system (including flow paths with different length and transit times) in a V-shape valley transect (A-A´ section; see location in Fig. 1B) of lowlands in the BRW. (B) Detailed geologic profile of the top 50 m of the crystalline basement (not at scale).

The main geochemical process identified in the groundwater samples are attributed to the processes of precipitation concentration through evapotranspiration and silicate weathering (i.e. mainly albite, anorthite, tremolite and K-feldspar hydrolysis), as expected due to the Na-K-Ca-Mg-rich mineralogical composition of Palaeozoic schists that crop out in the BRW. Therefore, a preferential geochemical evolution towards rCa/rMg enriched waters is generally observed in groundwater samples. The fact that HCO_3 is the main anion in most groundwater samples can be explained by the CO_2 dissolution from the soil/atmospheric air, which is needed to produce the chemical rock weathering processes (Gaillardet et al., 1999; Donnini et al., 2016).

Analysis of water temperature in the Bérchules River shows substantial differences in the altitudinal thermal gradient between air and surface water during winter (January-February sampling campaign; Fig. 6B), which is the direct consequence of the snow melt effect. In contrast, surface water collected during the May-June survey became warmer and more enriched in solutes as the sampled river stretch was progressively located downstream (Fig. 6B). This general warming of surface waters is attributed to the high proportion of groundwater that flows into the river during the spring-summer season, when the river flow upstream (headwaters) is mostly allocated to the *acequias de careo* system and the remaining channel network for aquifer recharge. Thus, the Bérchules River receives lateral inflows from the shallow metamorphic aquifer and behaves as a gaining river practically throughout its length during the dry season.

662 The results of this study also point to the effects of the ancient managed recharge system
663 on groundwater quality dynamics in the BRW. The aquifer zones influenced by recharge
664 coming from the *acequias de careo* are clearly distinguished by means of the isotopic
665 content of groundwater (Figs. 7 and 14). Firstly, the isotopic content of groundwater in
666 the springs not affected by the artificial recharge system shows a linear altitudinal
667 dependence with a gradient lower than the one corresponding to precipitation (i.e.
668 $\nabla_z \delta^{18}\mathrm{O}_{\mathrm{GROUNDWATER}} < \nabla_z \delta^{18}\mathrm{O}_{\mathrm{P}}$), as happens in the case of sloping aquifer recharge
669 (Custodio and Jódar, 2016). Secondly, the isotopic content of groundwater in the springs
670 influenced by the induced recharge does not show any relationship with elevation. This
671 reflects how snow melt water (i.e. isotopically lighter) flows through the *acequias de*
672 *careo* network towards lower altitude areas, where it finally infiltrates concentrated in
673 densely fractured zones. Therefore, groundwater drained by springs partially or totally
674 fed by recharged water from the *acequias de careo* network system is characterized by
675 lighter isotopic composition than would be expected according to its natural recharge
676 area. Isotope hydrology proves to be a powerful tool to delineate the aquifer zones fed
677 not only by rainfall/river recharge, but also by artificial recharge from the *acequias de*
678 *careo* system.

679 As stated in previous sections, recharge in the metamorphic aquifer was found to be
680 anomalously high. The recharge rate in the present study is quantified by means of the
681 chloride mass balance method as 15-20 % of rainfall. This estimation is coherent with the
682 results numerically obtained by Martos-Rosillo et al. (2017), Jódar et al. (2017) and Jódar
683 et al. (2018), who reported recharge estimates, as a percentage of mean annual
684 precipitation, of 19 ± 16 (using Visual-Balan code; Samper et al., 1999; 2005), 20 ± 11
685 (by applying Témez model; Témez, 1977; Jódar et al., 2017) and 25 ± 13 (using HBV
686 model; Bergström, 1976; Seibert, 2005), respectively. The use of environmental tracers

687 and numerical simulations seem to provide reliable recharge results in the BRW, even
688 taking into account that the aquifer (1) is hosted in metamorphic materials, and (2) is
689 located in a high mountain area with large altitudinal variations, where semiarid-arid
690 regional climate conditions prevail. Singhal and Gupta (2010) reported similar recharge
691 rates in hard-rock aquifers of subtropical areas, where rainfall is substantially higher than
692 in the BRW. The relatively high recharge rate calculated in the BRW can be also deduced
693 from the high groundwater contribution (83-97%) to the total river basin runoff at the
694 Narila gauging station (Figs. 1 and 2) obtained by Al-Awani (1997), Martos-Rosillo et al.
695 (2017), and Jódar et al. (2017; 2018). In short, the *acequias de careo* system causes the
696 aquifer recharge to be significantly higher than that obtained if only natural recharge had
697 occurred. This is the reason why in other basins of Sierra Nevada, where the *acequias de*
698 *careo* do not operate or do not exist, the number of springs and their duration, as well as
699 the basin base flow, are much lesser.

700 The *acequias de careo* system helps enhance the aquifer recharge and therefore increase
701 the role played by groundwater discharge in the total Bérchules River runoff.
702 Accordingly, Martos-Rosillo et al. (2015a) reported an infiltration volume of 2 hm^3 for
703 the hydrologic year 2015/2016 in El Espino canal (Fig. 1). This volume represents 40%
704 of the total river discharge measured at the Narila gauging station during that hydrologic
705 year. The recharge system furthermore produces a buffer effect in the Bérchules River
706 hydrograph (Fig. 2) by smoothing the discharge peak during the snow melt season while
707 increasing the river base flow during the dry season, coinciding with the critical water
708 demand that typically occurs in summer. This basin behavior is contrary to what might
709 be expected for high mountain rivers as a result of global warming (Barnet et al., 2005),
710 a scenario in which less precipitation will fall as snow, shifting both the melting season
711 and the rivers main discharge peak to earlier times, away from the water resource demand

712 period (Tague and Grant, 2009; Jenicek et al., 2018). If applied to other alpine basins
713 around the world, the *acequias de careo* recharge system would provide a valuable
714 adaptation strategy to mitigate the impact of the possible forecasted climate change in
715 these zones.

716

717 **6. Conclusions**

718 The *acequias de careo* is an ancient water management system developed in alpine zones
719 of southern Spain that provides water to downstream-depending users when the water
720 demand is highest. The ancient recharge system modifies the natural hydrological
721 dynamics of the basin by enhancing diffuse recharge up to 20% of precipitation, which is
722 a very substantial value taking into account the high slopes and the metamorphic nature
723 of the rocks conforming the basin.

724 Chemical weathering of silicate minerals and concentration of rainfall by
725 evapotranspiration are the key processes behind groundwater mineralization.
726 Additionally, groundwater from springs not affected by the *careo* recharge system shows
727 an altitudinal thermal gradient coinciding with that of the air temperature, and also an
728 isotopic vertical gradient lower than that of precipitation, a behavior typically associated
729 with sloping-recharge aquifers. Nevertheless, the managed recharge through the *acequias*
730 *de careo* modifies the physico-chemical and isotopic response of the springs affected by
731 the recharge system, by fading such altitudinal thermal and isotopic gradients.

732 The presence of the *acequias de careo* 1) makes the aquifer recharge significantly higher
733 than that obtained if only natural recharge had occurred, and 2) modifies the hydrologic
734 basin behavior by reducing the snowmelt discharge peak and increasing the base flow
735 during the low rainfall periods. This basin behavior is contrary to what could be expected

for high mountain rivers as a result of global warming. Therefore, if the *acequias de careo* water management system were applied in other alpine basins around the world, it would come to be a valuable adaptation strategy to mitigate the forecasted impact of climate change

The high topographic, thermal and pluviometry gradients prevailing in the study area contribute to the relevance of water temperature and stable isotope contents in water as tools to characterize the hydrological behavior of similarly high mountain basins.

7. Acknowledgements

This research was funded by the Environmental and Water Agency of Junta de Andalucía through the project *"Investigación hidrogeológica de acuíferos de alta montaña sometidos a explotación intensiva del agua subterránea. Cabecera de los ríos Grande de Bérchules y Mecina" (Ref. Num. 2422)* [Hydrogeological investigation of highly exploited high mountain aquifers. The Bérchules and Messina headwater basins]. The authors would like to thank the staff of the Sierra Nevada National Park, especially Francisco Javier Sánchez Gutierrez and Ignacio L. Henares Civantos, for their generous support. The authors thank Jean Louise Sanders by the language revision of the paper.

754 **References**

755 Alcalá, F.J., Custodio, E., 2014. Spatial average aquifer recharge through atmospheric
756 chloride mass balance and its uncertainty in continental Spain. Hydrol. Process., 28,
757 218–236. https://dx.doi.org/10.1002/hyp.9556

758 Alcalá, F.J., Custodio, E., 2015. Natural uncertainty of spatial average aquifer recharge
759 through atmospheric chloride mass balance in continental Spain. J. Hydrol., 524:
760 642–661. https://dx.doi.org/10.1016/j.jhydrol.2015.03.018

761 Aldaya, F., Martínez-García, E., Díaz de Federico, A., Puga, E., Navarro-Vilá, F., 1979.
762 Mapa geológico de España [*Geologic map of Spain*], 1:50.000. Hoja 1.042,
763 Lanjarón. IGME, Madrid.

764 Aldaya, F., Baena, J., Ewert, K., 1983. Mapa geológico de España [*Geologic map of*
765 *Spain*], 1:50.000. Hoja 1.043, Berja. IGME, Madrid.

766 Al Alwani, G., 1997. Hidrología e hidrogeología en la cuenca del río Guadalfeo.
767 Aplicación del Modelo HPSF para la simulación de nieve y balance hídrico
768 [Hydrology and hydrogeology in the Guadalfeo river basin. Application of the
769 HPSF Model for snow simulation and water balance]. Ph.D. Thesis. Department of
770 Geodynamics. Universidad de Granada, Granada, Spain.

771 Appelo, C., Postma, D., 2007. Geochemistry, groundwater and pollution (2nd ed.). Taylor
772 and Francis, Amsterdam. 634 pp.

773 Barnett, T.P., Adam, J.C., Lettenmaier, D.P., 2005. Potential impacts of a warming
774 climate on water availability in snow-dominated regions, Nature, 438(17), 303–
775 309. https://dx.doi.org/10.1038/nature04141

776 Beniston M., Diaz H.F., Bradley R.S., 1997. Climatic Change at High Elevation Sites:
777 An Overview. In: Diaz H.F., Beniston M., Bradley R.S. (Eds.) Climatic Change at
778 High Elevation Sites. Springer, Dordrecht. https://doi.org/10.1007/978-94-015-
779 8905-5_1

780 Bergström, S., 1976. Development and Application of a Conceptual Runoff Model For
781 Scandinavian Catchments, SMHI, Report No. RHO 7, Norrköping (134 pp.).

782 Castillo, A., Fideli, B., 2002. Algunas pautas del comportamiento hidrogeologico de rocas
783 duras afectadas por glaciarismo y periglaciarismo en Sierra Nevada (Espana),
784 Geogaceta, 32, 189–191. http://hdl.handle.net/10272/9131

785 Chen, Z., Hartmann, A., Wagener, T., Goldscheider, N., 2017. Dynamics of water fluxes
786 and storages in an Alpine karst catchment under current and potential future climate
787 conditions. Hydrol. Earth Syst. Sci. Discuss., https://doi.org/10.5194/hess-2017-
788 216

789 Clow, D.W., Schrott, L., Webb, R., Campbell, D.H., Torizzo, A., Dornblaser, M., 2003.
790 Ground water occurrence and contributions to streamflow in an alpine catchment,
791 Colorado Front Range. Ground Water, 41(7), 937-950.
792 https://doi.org/10.1111/j.1745-6584.2003.tb02436.x

793 Cras, A., Marc, V., Travi, Y., 2007. Hydrological behavior of sub-Mediterranean alpine
794 headwater streams in a badlands environment. J. Hydrol., 339, 130–144.
795 https://doi.org/10.1016/j.jhydrol.2007.03.004

796 Claasen, H.C., Reddy, M.M., Halm, D.R., 1986. Use of the chloride ion in determining
797 hydrologic-basin water budgets: A 3-year case study in the San Juan Mountains,

798 Colorado, USA. J. Hydrol., 85: 49–71. https://doi.org/10.1016/0022-
799 1694(86)90076-4

800 Craig, H., 1961. Isotopic variations in meteoric waters. Science, 133, 1702–1703.

801 Custodio E., 2010. Estimation of aquifer recharge by means of atmospheric chloride
802 deposition balance. Contributions to Science, 6: 81–97.
803 https://doi.org/10.2436/20.7010.01.86

804 Custodio, E., Llamas, M.R. (Eds.), 1976/1983. Hidrología subterránea [Groundwater
805 hydrology]. 2 Vols: 1–2350. Ediciones Omega, Barcelona.

806 Custodio, E., Jódar, J., 2016. Simple solutions for steady–state diffuse recharge
807 evaluation in sloping homogeneous unconfined aquifers by means of atmospheric
808 tracers. J. Hydrol., 540, 287–305. https://dx.doi.org/10.1016/j.jhydrol.2016.06.035

809 Custodio, E., Jódar, J., Herrera, C., Custodio-Ayala, J., Medina, A., 2018. Changes in
810 groundwater reserves and radiocarbon and chloride content due to a climate dry-
811 wet-dry period sequence in a large unconfined aquifer in an arid area. J. Hydrol.,
812 556 (2018) 427–437. https://doi.org/10.1016/j.jhydrol.2017.11.035

813 D'Agata, C., Bocchiola, D., Maragno, D., Smiraglia, C., Diolaiuti, G.A., 2014. Glacier
814 shrinkage driven by climate change during half a century (1954–2007) in the Ortles-
815 Cevedale group (Stelvio National Park, Lombardy, Italian Alps). Theor. Appl.
816 Climatol., 116: 169. https://doi.org/10.1007/s00704-013-0938-5

817 Delaigue, M.C., 1995. La red de acequias de la Alpujarra Alta. In: El Agua en la
818 Agricultura de Al-Andalus. Ed. Fundación el Legado Andalusí- Lunwerg Editores
819 S. A. Madrid, España, 143–150.

Dettinger, M.D., 1989. Reconnaissance estimates of natural recharge to desert basins in Nevada, U.S.A., by using chloride-balance calculations. J. Hydrol., 106: 55–78. https://doi.org/10.1016/0022-1694(89)90166-2

Donnini, M., Frondini, F., Probst, J.L., Probst, A., Cardellini, C., Marchesini, I., Guzzetti, M., 2016. Chemical weathering and consumption of atmospheric carbon dioxide in the Alpine region. Glob. Planet Change, 136 65–81. https://doi.org/10.1016/j.gloplacha.2015.10.017

Eriksson, E., 1960. The yearly circulation of chloride and sulphur in nature; meteorological, geochemical and pedological implications, part II. Tellus, 12, 63–109. https://doi.org/10.3402/tellusa.v12i1.9341

Eriksson, E., Khunakasen, V., 1969. Chloride concentrations in groundwater, recharge rate and rate of deposition of chloride in the Israel coastal plain. J. Hydrol., 7 (2), 178–197. https://doi.org/10.1016/0022-1694(69)90055-9

Fernández-Chacón, F., Benavente, J., Rubio-Campos, J.C., Kohfahl, C., Jiménez, J., Meyer, H., Hubberten, H., Pekdeger, A., 2010. Isotopic composition (δ18O and δD) of precipitation and groundwater in a semi-arid, mountainous area (Guadiana Menor basin, Southeast Spain). Hydrol Process, 24:1343–1356. https://doi.org/10.1002/hyp.7597

Fraser, B., 2012. Melting in the Andes: goodbye glaciers. Nature, 491, 180–182. https://doi.org/10.1038/491180a

Gaillardet, J., Dupré, B., Louvat, P., Allègre, C.J., 1999. Global silicate weathering and CO2 consumption rates deduced from the chemistry of large rivers. Chem. Geol., 159, 3–30. https://doi.org/10.1016/S0009-2541(99)00031-5

Gómez-Ortiz, A., Palacios, D., Palade, B., Vázquez-Selem, L., Salvador_Franch, F., 2012. The deglaciation of Sierra Nevada (Southern Spain). Geomorphology, 159-160, 93-105. https://doi.org/10.1016/j.geomorph.2012.03.008

Gómez-Ortiz, A., Oliva, M., Palacios, D., Salvador-Franch, F, Vázquez-Selem, L., Salvá-Catarineu, M. and De Andrés, N., 2015. The deglaciation of Sierra Nevada (Spain). Synthesis of the knowledge and new contributions. Cuadernos de Investigación Geográfica, 41(2), 409–426. https://doi.org/10.18172/cig.2722

Gómez-Zotano, J., Alcántara-Manzanares, J., Olmedo-Cobo, J.A., Martínez-Ibarra, E., 2015. La sistematización del clima mediterráneo: identificación, clasificación y caracterización climática de Andalucía (España) [The systematization of the Mediterranean climate: identification, classification and climatic characterization of Andalusia (Spain)]. Revista de Geografía Norte Grande 61:161–180. https://dx.doi.org/10.4067/S0718-34022015000200009

González-Ramón, A., Moral-Martos, F., Marín-Lechado, C., Martos-Rosillo, S., Pedrera-Parias, A., Ruiz-Constan, A., Durán-Valsero, J.J., 2015. Factores geomorfológicos condicionantes de la hidrogeología de la cuenca alta del Río Bérchules (Sierra Nevada, Granada) [Geomorphological factors conditioning the hydrogeology of the upper basin of the Bérchules River (Sierra Nevada, Granada)]. Proceedings of SIAGA 2015, IGME editions.

Hargreaves, G.H., 1994. Defining and using reference evapotranspiration. J. Irrig. Drain. Eng., 120 (6):1132–1139. https://dx.doi.org/10.1061/(ASCE)0733-9437(1994)120:6(1132)

Herrera, C., Custodio, E., Chong, G., Lambán, L.J., Riquelme, R., Wilke, H., Jódar, J., Urrutia, J., Urqueta, H., Sarmiento, A., 2016, Groundwater flow in a closed basin

with a saline shallow lake in a volcanic area: Laguna Tuyajto, northern Chilean Altiplano of the Andes. Sci. Total Env., v. 541, p. 303–318. http://dx.doi.org/10.1016/j.scitotenv.2015.09.060

Hood, J.L., Roy, J.W., Hayashi, M., 2006. Importance of groundwater in the water balance of an alpine headwater lake. Geophys. Res. Lett., 33, L13405. http://dx.doi.org/10.1029/2006GL026611

Hood, J.L., Hayashi, M., 2015. Characterization of snowmelt flux and groundwater storage in an alpine headwater basin. J. Hydrol., 521:482–497. https://doi.org/10.1016/j.jhydrol.2014.12.041

Huth, A.K., Leydecker, A., Sickman, J.O., Bales, R.C., 2004. A two-component hydrograph separation for three high-mountain catchments in the Sierra Nevada, California. Hydrol. Process., 18, 1721–1733. https://doi.org/10.1002/hyp.1414

Immerzeel, W.W., van Beek, L.P.H., Bierkens, M.F.P., 2010. Climate change will affect the Asian water towers, Science, 328, 1382–1385, 2010. https://doi.org/10.1126/science.1183188

Jenicek, M., Seibert, J., Staudinger, M., 2018. Modeling of future changes in seasonal snowpack and impacts on summer low flows in alpine catchments. Water Resour. Res., 54. https://doi.org/10.1002/2017WR021648

Jiménez-Gavilán, P., 2010. Caracterización hidrogeológica de acuíferos carbonáticos del sur de España a partir de sus respuestas naturales [Hydrogeological characterization of carbonate aquifers in southern Spain based on their natural responses]. Ph.D. Thesis, Universidad de Granada, Granada, Spain. http://hdl.handle.net/10481/5641

889 Jódar, J., Custodio, E., Lambán, L.J., Martos-Rosillo, S., Herrera-Lameli, C., Sapriza-
890 Azuri, G., 2016. Vertical variation in the amplitude of the seasonal isotopic content
891 of rainfall as a tool to jointly estimate the groundwater recharge zone and transit
892 times in the Ordesa and Monte Perdido National Park aquifer system, north-eastern
893 Spain. Sci. Total Environ., 573, 505–517.
894 https://dx.doi.org/10.1016/j.scitotenv.2016.08.117

895 Jódar, J., Cabrera, J.A., Martos-Rosillo, S., Ruiz-Constán, A., González-Ramón, A.,
896 Lambán, L.J., Herrera, C., Custodio, E., 2017. Groundwater discharge in high-
897 mountain watersheds: A valuable resource for downstream semi-arid zones. The
898 case of the Bérchules River in Sierra Nevada (Southern Spain). Sci. Total Env.,
899 593-594, 760–772. https://dx.doi.org/10.1016/j.scitotenv.2017.03.190

900 Jódar, J., Carpintero, E., Martos-Rosillo, S., Ruiz-Constán, A., Marín-Lechado, C.,
901 Cabrera-Arrabal, J.A., Navarrete-Mazariegos, E., González-Ramón, A., Lambán,
902 L.J., Herrera, C., González-Dugo, M.P., 2018. Combination of lumped hydrological
903 and remote-sensing models to evaluate water resources in a semi-arid high altitude
904 ungauged watershed of Sierra Nevada (Southern Spain). Sci. Total Env., 625 (2018)
905 285–300. https://doi.org/10.1016/j.scitotenv.2017.12.300

906 Kahn, K.G., Ge, S., Caine, J.S., Manning, A., 2008. Characterization of the shallow
907 groundwater system in an alpine watershed: Handcart Gulch, Colorado, USA.
908 Hydrogeol. J., 16(1), 103–121. https://doi.org/10.1007/s10040-007-0225-6

909 Lambán, L.J., Jódar, J., Custodio, E., Soler, A., Sapriza, G., Soto, R., 2015. Isotopic and
910 hydrogeochemical characterization of high-altitude karst aquifers in complex
911 geological settings. The Ordesa and Monte Perdido National Park (Northern Spain)

912 case study. Sci. Total Env., 506–507: 466–479.
913 https://dx.doi.org/10.1016/j.scitotenv.2014.11.030

914 Langston, G., Hayashi, M., Roy, J.W., 2013. Quantifying groundwater–surface water
915 interactions in a proglacial moraine using heat and solute tracers. Water Resour.
916 Res., 49:5411–5426. https://dx.doi.org/10.1002/wrcr.20372

917 Lauber, U., Goldscheider, N., 2014. Use of artificial and natural tracers to assess
918 groundwater transit-time distribution and flow systems in a high-alpine karst
919 system (Wetterstein Mountains, Germany). Hydrogeol. J., 22: 1807–1824.
920 https://doi.org/10.1007/s10040-014-1173-6

921 Lauber, U., Kotyla, P., Morche, D., Goldscheider, N., 2014. Hydrogeology of an Alpine
922 rockfall aquifer system and its role in flood attenuation and maintaining baseflow.
923 Hydrol. Earth Syst. Sci., 18, 4437–4452, https://doi.org/10.5194/hess-18-4437-
924 2014

925 Liu, F.J., Parmenter, R., Brooks, P.D., Conklin, M.H., Bales, R.C., 2008. Seasonal and
926 interannual variation of streamflow pathways and biogeochemical implications in
927 semi-arid, forested catchments in Valles Caldera, New Mexico. Ecohydrology. 1
928 (3), 239–252. https://doi.org/10.1002/eco.22

929 Liu, F.J., Williams, M.W., Caine, N., 2004. Source waters and flow paths in an alpine
930 catchment, Colorado Front Range, United States. Water Resour. Res., 40 (9).
931 https://doi.org/10.1029/2004WR003076

932 Locutura, J., Bel-lan A., García-Cortés, A., Martínez, S., 2012. Atlas Geoquímico de
933 España. Publicado por IGME (Instituto Geológico y Minero de España) ISBN: 978-
934 84-7840-875-7. 592 pag. Madrid.

935 Martín-Civantos, J.M., 2007. Poblamiento y territorio medieval en el Zenete, Granada
936 [Settlement and medieval territory in the Zenete, Granada]. Granada: Universidad
937 de Granada. 773 pp.

938 Martos-Rosillo, S., González-Ramón, A., Rodríguez Rodríguez, F., Marín, C., Guardiola-
939 Albert, C., Durán, J.J., Fernández, L., Navarrete, E., López-Rodríguez, M.,
940 Fernández, M., Rodríguez-Rodríguez, M., Bruque, J.M., Ruiz-Costán, A., Pedrera,
941 A., 2015a. ¿Tiene interés hidrogeológico preservar las acequias de carero de Sierra
942 Nevada? El caso de la acequia de careo de El Espino (Río Bérchules, Granada)
943 [Does it make sense from a hydrogeological point of view to preserve the irrigation
944 canals of the Sierra Nevada? The case of the irrigation channel of El Espino
945 (Bérchules River, Granada)]. Proceedings of SIAGA 2015, IGME editions.

946 Martos-Rosillo, S., Guardiola-Albert, S., Marín-Lechado, S., González-Ramón, A.,
947 Villagómez, B., Peregrina, M., Fernández, L., Durán, J.J., Navarrete, E., López-
948 Rodríguez, M., Pedrera, A., Ruiz-Costán, A., Cabrera, J.A., 2015b. Caracterización
949 hidrogeológica y evaluación de la recarga de un acuífero de alta montaña
950 desarrollado en rocas duras. Cuenca del río Bérchules. Sierra Nevada. Granada
951 [Hydrogeological characterization and recharge evaluation of high mountain
952 aquifers developed in hard rocks. Bérchules river basin. Sierra Nevada. Granada].
953 Proceedings of SIAGA 2015, IGME editions.

954 Martos-Rosillo, S., González-Ramón, A., Marín-Lechado, C., Cabrera, J.A., Guardiola-
955 Albert, C., Jódar, J., Navarrete, E., Ruiz-Constán, A., Moral, F., Pedrera, A., Navas,
956 R., López, M., Durán, J.J., 2017. Las acequias de careo de Sierra Nevada (Sur de
957 España), un sistema de recarga ancestral en acuíferos de alta montaña [The *acequias*
958 *de careo* of Sierra Nevada (Southern Spain), an ancestral recharge system in high

959 mountain aquifers]. In: Óscar Escolero, Carlos Gutiérrez and Edgar Mendoza (Eds.)
960 Manejo de la recarga de acuíferos. 527–563. Instituto Mexicano de Tecnología del
961 Agua (IMTA).

962 McClymont, A.F., Hayashi, M., Bentley, L.R., Muir, D., Ernst, E., 2010. Groundwater
963 flow and storage within an alpine meadow-talus complex. Hydrol. Earth Syst. Sc.,
964 14(6), 859–872. https://doi.org/10.5194/hess-14-859-2010

965 McClymont, A.F., Hayashi, M., Bentley, L.R., Liard, J., 2012. Locating and
966 characterising groundwater storage areas within an alpine watershed using time-
967 lapse gravity, GPR and seismic refraction methods. Hydrol. Process., 26: 1792–
968 1804. https://doi.org/10.1002/hyp.9316

969 Messerli, B., Viviroli, D., Weingartner, R., 2004. Mountains of the world: vulnerable
970 water towers for the 21st century. Ambio, 13:29–34.
971 https://www.jstor.org/stable/25094585

972 Meybeck, M., Green, P., Vörösmarty, C.J., 2001. A new typology for mountains and other
973 relief classes: An application to global continental water resources and population
974 distribution, Mt Res Dev, 21(1), 34–45. https://doi.org/10.1659/0276-
975 4741(2001)021[0034:ANTFMA]2.0.CO;2

976 Molina, A.J., Latron, J., Rubio, C.M., Gallart, F., Llorens, P., 2014. Spatio-temporal
977 variability of soil water content on the local scale in a Mediterranean mountain area
978 (Vallcebre, North Eastern Spain). How different spatio-temporal scales reflect
979 mean soil water content. J. Hydrol., 516:182–192.
980 https://dx.doi.org/10.1016/j.jhydrol.2014.01.040

Moore, R.D., Fleming, S.W., Menounos, B., Wheate, R., Fountain, A., Stahl, K., Holm, K., Jakob, M., 2009. Glacier change in western North America: influences on hydrology, geomorphic hazards and water quality. Hydrol. Process., 23, 42–61, https://doi.org/10.1002/hyp.7162

Parkhurst, D., Appelo, C., 1999. User's guide to PHREEQC (version 2) - A computer program for speciation, batch-reaction, one-dimensional transport, and inverse geochemical calculations. Water Resources Research Investigations Report 99-4259, 326 p.

Pulido-Bosch, A., Sbih, Y., 1995. Centuries of artificial recharge on the southern edge of the Sierra Nevada (Granada, Spain). Environ. Geol., 26, 57–63. https://doi.org/10.1007/BF00776033

Raya Garrido, J., 2003. Composición isotópica del vapor de agua atmosférico en el sureste de la Península Ibérica [Isotopic composition of atmospheric water vapor in the southeast of the Iberian Peninsula]. Ph.D. Thesis, Universidad de Granada, Granada, Spain. http://hdl.handle.net/10481/1756

Roy, J.W., Hayashi, M., 2009. Multiple, distinct groundwater flow systems of a single moraine-talus feature in an alpine watershed. J. Hydrol., 373, 139–150. https://doi.org/10.1016/j.jhydrol.2009.04.018

Sami, K., Hughes, D.A., 1996. A comparison of recharge estimates to a fractured sedimentary aquifer in South Africa from a chloride mass balance and an integrated surface-subsurface model. J. Hydrol., 179: 111–136. https://doi.org/10.1016/0022-1694(95)02843-9

1003 Samper, J., Huguet, L., Arés, J., García, M.A. 1999. Manual del usuario del Programa
1004 Visual Balan: V. 1.0. Código interactivo para la realización de balances
1005 hidrológicos y la estimación de la recarga [User Manual of the Visual Balan
1006 Program: V. 1.0. Interactive code for the realization of hydrological balances and
1007 aquifer recharge estimation]. Empresa Nacional de los Residuos Radioactivos,
1008 ENRESA, Madrid, 132 pp.

1009 Samper, J., Huguet, L., Ares, J. y García-Vera, M.A. 2005. Manual del Usuario del
1010 programa VISUAL BALAN v.2.0 [User Manual of the VISUAL BALAN v.2.0
1011 program]. Editorial, ENRESA, Madrid. 139 p.

1012 Scanlon, B.R., Keese, K.E., Flint, A.L., Flint, L.E., Gaye, C.B., Edmunds, W.M.,
1013 Simmers, I., 2006. Global synthesis of groundwater recharge in semiarid and arid
1014 regions. Hydrol. Process, 20: 3335–3370. https://doi.org/10.1002/hyp.6335

1015 Scherler, D., Bookhagen, B., Strecker, M.R., 2011. Spatially variable response of
1016 Himalayan glaciers to climate change affected by debris cover, Nat. Geosci., 4,
1017 156–159. https://doi.org/10.1038/NGEO1068

1018 Seibert, J., 2005. HBV Light Version 2. User's Manual. Uppsala University, Dept. of
1019 Earth Science, Hydrology, Uppsala, Sweden.

1020 Singhal, B., Gupta, R., 2010. Applied Hydrogeology of Fractured Rocks. 2nd ed. Springer
1021 Netherlands. https://doi.org/10.1007/978-90-481-8799-7

1022 Taylor, R.G., Scanlon, B., Doll, P., Rodell, M., van Beek, R., Wada, Y., Longuevergne,
1023 L., Leblanc, M., Famiglietti, J.S., Edmunds, M., Konikow, L., Green, T.R., Chen,
1024 J., Taniguchi, M., Bierkens, M.F.P., MacDonald, A., Fan, Y., Maxwell, R.M.,
1025 Yechieli, Y., Gurdak, J.J., Allen, D.M., Shamsudduha, M., Hiscock, K., Yeh, Pat

J.-F., Holman, I., Treidel, H., 2012. Ground water and climate change. Nat. Clim. Chang., 3 (4): 322–329. https://dx.doi.org/10.1038/nclimate1744

Viviroli, D., Archer, D.R., Buytaert, W., Fowler, H.J., Greenwood, G.B., Hamlet, A.F., Huang, Y., Koboltschnig, G., Litaor, M.I., Lopez-Moreno, J.I., Lorentz, S., Schadler, B., Schreier, H., Schwaiger, K., Vuille, M., Woods, R., 2011. Climate change and mountain water resources: overview and recommendations for research, management and policy. Hydrol. Earth Syst. Sci., 15, 471–504. https://doi.org/10.5194/hess-15-471-2011

Viviroli, D., Dür, H.H., Messerli, B., Meybeck, M., Weingartner, R., 2007. Mountains of the world, water towers for humanity: topology, mapping and global significance. Water Resour. Res., 43, W07447. https://dx.doi.org/10.1029/2006WR005653

Wood, W.W., 1999. Use and misuse of the chloride–mass balance method in estimating ground water recharge. Ground Water, 37 (1), 2–3. https://dx.doi.org/10.1111/j.1745-6584.1999.tb00949.x

Wood W.W., Sanford W.E., 1995. Chemical and isotopic methods for quantifying ground-water recharge in a regional, semiarid environment. Ground Water, 33, pp. 458–468. https://dx.doi.org/10.1111/j.1745-6584.1995.tb00302.x